Article:
Li, D., Hu, M., Chen, H. et al. (9 more authors) (2022) An Nphp1 knockout mouse model targeting exon 2–20 demonstrates characteristic phenotypes of human Nephronophthisis. Human Molecular Genetics, 31 (2). pp. 232-243. ISSN 0964-6906

https://doi.org/10.1093/hmg/ddab239

Title: An *Nphp1* Knockout Mouse Model Targeting Exon 2-20 Demonstrates Characteristic Phenotypes of Human Nephronophthisis

Authors:

Dantong Li[1,+], Miaoyue Hu[2,+], Huamu Chen[1], Xiaohong Wu[1], Xiaoya Wei[1], Hongrong Lin[1], Xuefei Gao[3], Haiyan Wang[4], Min Li[1], Albert C.M. Ong[5], Zhihui Yue[2,*], Liangzhong Sun[1,*]

Author Affiliation:

1. Department of Pediatrics, Nanfang Hospital, Southern Medical University, Guangzhou 510515, China.

2. Department of Pediatrics, The First Affiliated Hospital, Sun Yat-sen University, Guangzhou 510080, China

3. Department of Physiology, School of Basic Medical Sciences, Southern Medical University, Guangzhou, China.

4. Department of Pediatrics, Sun Yat-sen Memorial Hospital, Sun Yat-sen University, Guangzhou 510120, China.

5. Kidney Genetics Group, Academic Nephrology Unit, Department of Infection, Immunity and Cardiovascular Disease, University of Sheffield Medical School, Sheffield, UK.

Correspondence to:

Dr. Liangzhong Sun, Department of Pediatrics, Nanfang Hospital, Southern Medical University, No. 1838, North Road, Guangzhou Avenue, Baiyun District, Guangzhou 510515, Guangdong, China. Email address: sunlzh2018@smu.edu.cn; Tel.: 0086 13316202736; Fax: 0086 20 8770 3645.

Dr. Zhihui Yue, Department of Pediatrics, the First Affiliated Hospital, Sun Yat-sen University, 58 courtyard, Zhongshan Road II, Yuexiu District, Guangzhou 510080, Guangdong, China. Email address: yuezhh@mail.sysu.edu.cn; Tel.: 0086 13380029136; Fax: 0086 20 8775 0632.

[+]These authors contribute equally to this research.

Abstract

Nephronophthisis (NPH) is the most prevalent monogenetic disorder leading to end-stage renal failure (ESRD) in childhood. Mutations in *Nphp1*, encoding a cilia-localized protein, account for the majority of NPH cases. Despite its identification many years ago, *Nphp1* deletions targeting exon 4 or exon 20 have not reproduced the histological features of human NPH in murine models. In this study, we deleted exon 2-20 of *Nphp1* by CRISPR/Cas9 gene editing to create a near-total knockout (KO) mouse model (*Nphp1*$^{del2\text{-}20/del2\text{-}20}$). *Nphp1*$^{del2\text{-}20/del2\text{-}20}$ mice faithfully reproduced the renal and extrarenal phenotypes associated with human NPH, including renal cyst development, tubular basement membrane thickening, retinal degeneration and abnormal spermatogenesis. Importantly, *Nphp1* re-expression using an adenoviral-associated-virus-9 (AAV9) vector could partially rescue both renal and retinal phenotypes in *Nphp1*$^{del2\text{-}20/del2\text{-}20}$ mice. Our results reported the first relevant *Nphp1* mouse model with renal phenotypes for human disease. It will be a valuable model for future studies of *Nphp1* function and to develop novel treatments for this common childhood disease.

Introduction

Nephronophthisis (NPH, OMIM: 256100) is an important genetic cause of end-stage renal disease (ESRD) in children and young adults, accounting for 2.4% to 15% of pediatric ESRD cases (1,2,3). It shows an autosomal recessive inheritance pattern with an estimated incidence of 1:50 000 (4). The clinical presentation as well as the genetic background are highly variable. NPH can be either isolated or associated with different extra-renal manifestations (ophthalmic symptoms, liver fibrosis, neurologic disorders, etc.) (5,6). Although mutations have been identified in more than 20 different genes (*Nphp1* to -20; *IFT1*40) so far (7,8,9,10), the most frequent NPHP mutation is a homozygous deletion of *Nphp1*, which is found in approximately 27%-62% of NPH patients (6).

Nephrocystin-1, the protein encoded by *Nphp1*, localizes to the primary cilium and is widely expressed in many tissues (11). To gain insight into the physiological function of nephrocystin-1, several *Nphp1*-targeted mutant murine models have been generated. A *Nphp1* exon 20-deleted ($Nphp1^{del\ 20/del20}$) mouse model was produced by Cre-lox P recombination but this model did not recapitulate human NPH (12). A second mouse model with targeted disruption of *Nphp1* by insertion of a neo-bpA cassette in exon 4, developed gradual retinal degeneration without typical NPH renal features (13). Finally, a bacterial artificial chromosome (BAC)-transgenic model was created using the human *NPHP1* locus (chromosome 2q13). This transgenic model mirrored neurodevelopmental disorders in humans with a 2q13 duplication but did not

report the kidney findings (14).

Thus, no murine *Nphp1* models which reproduces the human NPH kidney phenotype have been reported so far. These results might be explained by the complex protein structure and uncertain functions of nephrocystin-1. Secondary structure predictions of nephrocystin-1 from N-terminal to C-terminal are: coiled-coil domains encoded by exon 1-4, first E-rich domain encoded by exon 5, SH3 domain encoded by exon 5-6, second E-rich domain encoded by exon 7, and a conserved nephrocystin homology domain that encompasses the C-terminal two thirds of the protein. The SH3 domain encoded by exon 5-6 of *Nphp1* is the most notable structural motif as a protein-protein interaction module capable of binding multiple proteins with proline-rich sequences (15,16,17,18). We hypothesized that to generate a *Nphp1* null allele, exon 5-6 encoding the SH3 domain must be deleted. However, in a previous study, DNA fragments flanking exon 5–6 were found to be inefficient arms for homologous recombination in mouse embryonic stem cells and failed to generate either a null or hypomorphic allele (12). Considering that 80% of patients with *Nphp1* mutations harbor large homozygous gene deletions, deletion of large-scale *Nphp1* could be an alternative strategy (19). Since exon 1 is close to T cell differentiation protein (*Mtln*) and mitotic checkpoint serine/threonine kinase (*Bub1*) (14), we decided to delete exon 2-20 of the murine locus (sparing exon 1) by CRISPR/Cas9 gene editing.

In this paper, we report that this model, *Nphp1*$^{del2\text{-}20/del2\text{-}20}$, developed both renal and extrarenal characteristics of human NPH, and could be partially rescued by

re-expressing *Nphp1* in an adeno-associated-viral vector (*Nphp1*-OE). To our knowledge, the *Nphp1*$^{del2\text{-}20/del2\text{-}20}$ mouse is the first *Nphp1* model which faithfully reproduces human NPH.

Results

Generation and characterization of *Nphp1*$^{del2\text{-}20/del2\text{-}20}$ mice

Co-injection of single guide RNAs (sgRNAs) targeting exon 2-20 (Table S1a) and Cas9 protein was performed in C57BL/6J eggs. Mice carrying mosaic heterozygous indel modifications were confirmed by Sanger sequencing (Table S1b). 10 most likely off-target sites of each sgRNA were tested (Table S1c). Founder mice were then backcrossed to wild-type C57BL/6J mice to generate *Nphp1*$^{+/del2\text{-}20}$ mice. We focused on the mouse line carrying a 6 bp deletion and a 39 796 bp deletion in exon 2-20 (Figure 1a). Intercross of this mouse line (*Nphp1*-q) produced offspring at expected Mendelian ratio (1.1:1:1.9), indicating no embryonic lethality of homozygous indels (Figure 1b). PCR-based genotyping indicated that *Nphp1*$^{del2\text{-}20/del2\text{-}20}$ mice contained exon 2-20 deletion alleles (Figure 1c). To confirm whether the deletion of exon 2-20 inactivated the *Nphp1* gene, we determined the expression of *Nphp1* mRNA and protein in *Nphp1*$^{del2\text{-}20/del2\text{-}20}$ mice (Figure 1d-e).

Nphp1$^{del2\text{-}20/del2\text{-}20}$ mice recapitulate the renal phenotype of human NPH

In previous clinical studies (20,21) including our own (22), the renal ultrasound

findings of NPH patients revealed normal or smaller kidneys. Histologically, corticomedullary cyst formation, atrophy of renal tubular structure, tubular basement membrane thickening or disintegration and tubulointerstitial fibrosis are the hallmarks of NPH (23). Consistent with clinical data, renal size of 36 or 72-week-old *Nphp1*$^{del2\text{-}20/del2\text{-}20}$ mice were not visibly altered compared to *Nphp1*$^{+/+}$ mice and the kidney-to-body weight ratio (KW/BW) of these groups were not significantly different (Figure 2a-b). A non-significant but lower trend of serum urea and creatinine concentrations were shown in 12-week-old *Nphp1*$^{del2\text{-}20/del2\text{-}20}$ mice (Figure S1a-b). However, an increase in 24h-urine output and a decrease in urine specific gravity were observed in 5-week-old *Nphp1*$^{del2\text{-}20/del2\text{-}20}$ mice (Figure S1c-d), indicating impaired tubular urine concentrating capacity. These changes became much more prominent in 8-week-old mice (Figure 2c-d). Renal histology in *Nphp1*$^{del2\text{-}20/del2\text{-}20}$ mice showed the characteristic features of NPH. At the cortico-medullary junction, there were multiple cysts of different sizes (Figure 2e, iii and iv; 2f, iv, cy). Hypertrophied tubules were evident (Figure 2f, iii, dt). Segmental thickening and layering of tubular basement membranes could be observed (Figure 2f, vii and viii; 2g, ii, arrow). Tubulointerstitial fibrosis was unremarkable in 12-week-old *Nphp1*$^{del2\text{-}20/del2\text{-}20}$ mice (data not shown), but fibrotic changes could be seen by 36 weeks (Figure 2f, xi and xii) and became much more prominent by 72 weeks (Figure 2h, iii and iv). Fibrosis score was calculated in 72-week-old mice kidneys (Figure 2i). Glomerulosclerosis was present in 72-week-old *Nphp1*$^{del2\text{-}20/del2\text{-}20}$ mice when compared to the control group, indicated by poorer vascular patency and

periglomerular fibrosis (Figure S1e). Renal function of 72-week-old *Nphp1*$^{del2\text{-}20/del2\text{-}20}$ mice also showed a significant elevation in serum urea or creatinine concentrations (Figure 2j and 2k). Although all the experiments conducted above were focused on the mouse line *Nphp1-q*, similar renal phenotypes with cyst formation or tubular dilation could also been observed in line *Nphp1-r* and *Nphp1-s* (Figure S1f).

Re-expressing *Nphp1* in *Nphp1*$^{del2\text{-}20/del2\text{-}20}$ mice reversed the cystic renal phenotype

To see if the renal phenotypes could be rescued after *Nphp1* re-expression, *Nphp1* was systemically administrated into 5-week-old *Nphp1*$^{del2\text{-}20/del2\text{-}20}$ (KO) mice using AAV9 containing over-expression (OE) vectors (Figure 3a). Adenovirus vector without *Nphp1* served as a negative control (Vec). No alterations in kidney size or body weight were observed after delivery of either AAV9-OE or AAV-Vec (Figure 3b-d). *Nphp1* was re-expressed in KO mice at mRNA and protein levels (Figure 3e-g). IF staining of kidney sections demonstrated that nephrocystin-1 was mainly distributed at the apical surface of tubules (Figure 3g). Treatment with AAV-OE in 5-week-old *Nphp1*$^{del2\text{-}20/del2\text{-}20}$ mice led to a significant amelioration of cyst formation. The extent of tubular dilation was also greatly reduced (Figure 3h, vii and viii; 3i, vi and xii), with not visible thickening or layering of the tubular basement membrane (Figure 3i, xii and xvi). Tubulointerstitial fibrosis was improved in 36-week-old *Nphp1*$^{del2\text{-}20/del2\text{-}20}$ mice (Figure 3j, vi) when compared with their controls (Figure 3j, v). Accordingly, we also observed an improvement of glomerulosclerosis after

AAV-OE treatment in 36-week-old *Nphp1*$^{del2\text{-}20/del2\text{-}20}$ mice (Figure S2a, vi), along with the ameliorated monocyte infiltration (Figure S2b, vi). Additionally, the tubular urine concentrating capacity was improved in 8-week-old mice with AAV-OE treatment, as indicated by a decrease in 24h-urine output (Figure 3k) and an increase in urine specific gravity (Figure 3l). However, no significant alterations regarding kidney function could be measured in 36-week-old *Nphp1*$^{del2\text{-}20/del2\text{-}20}$ mice before or after AAV-OE treatment (Figure S2c-d), likely attributed to the mild TIF in 36-week-old mice. Fibroblast-specific protein 1 (FSP-1) and α-smooth muscle actin (α-SMA) are two markers of profibrotic cells (24), whose expression were clearly (FSP-1) or partly (α-SMA) stimulated in *Nphp1*$^{del2\text{-}20/del2\text{-}20}$ mice but downregulated after re-expression of *Nphp1* (Figure 3m-n).

Deleting exon2-20 of *Nphp1* induces retinal degeneration and spermatogenic defects, which can be partially reversed by *Nphp1* re-expression

The outer segment of photoreceptors (OS), inner segment of photoreceptors (IS), outer nuclear layer with photoreceptor cell nuclei (ONL), outer plexiform layer (OPL), inner nuclear layer (INL), inner plexiform layer (IPL) and ganglion cell layer (GCL) were all apparently visible in the retina of 12-week-old *Nphp1*$^{+/+}$ mice (Figure 4b, i). In the retina of *Nphp1*$^{del2\text{-}20/del2\text{-}20}$ mice, the OS, IS and ONL layers were completely absent, with hardly any existing OPL. Due to the severely abnormal OPL, the arrangement of INL was disorganized and its compactness disappeared (Figure 4b, iv).

After re-expression of nephrocystin-1 (Figure 4a), only a minor restoration of INL was observed, as characterized by an increased number of nuclei and partially improved compactness (Figure 4b, vi). The loss of OS, IS and ONL was not reversed by AAV-OE treatment at 5 weeks of age.

At the early stages of breeding, we failed to obtain *Nphp1*$^{del2\text{-}20/del2\text{-}20}$ mice by intercrossing existing male and female homozygous knockout mice. Our data showed that the testis weights of 12-week-old *Nphp1*$^{del2\text{-}20/del2\text{-}20}$ males were comparable with those of their control littermates (Figure 4c). In *Nphp1*$^{del2\text{-}20/del2\text{-}20}$ testes however, the hierarchical structure of the seminiferous tubule disappeared. The number of spermatogonia (sg), spermatocytes (sc), as well as spermatids (rs or est) were reduced. Instead, degenerated spermatogenic cells sloughed off into the lumen of seminiferous tubules. Elongating spermatids (est) sporadically existed, with bizarre heads, and usually no or only rudimentary tails, indicating an incomplete maturation process (Figure 4e, iv). We investigated if the re-expression of *Nphp1* at 5 weeks old could attenuate the testicular phenotypes. However, qPCR from whole testis lysates detected almost no re-expression of *Nphp1* (Figure 4d). The structure of the germinal epithelium remained disorganized indicating no rescue (Figure 4e, vi).

Data about skeletal and cardiac phenotypes were also provided. Body length of 5, 12, 36 and 72-week-old mice presented non-significant difference between *Nphp1*$^{+/+}$ and *Nphp1*$^{del2\text{-}20/del2\text{-}20}$ mice in both genders (Figure S3a-b). The tibia length of *Nphp1*$^{del2\text{-}20/del2\text{-}20}$ mice was close to that of the control group (Figure S3c). No polydactyly or dextrocardia was observed in 108 *Nphp1*$^{del2\text{-}20/del2\text{-}20}$ mice.

Microstructure of the heart was also exhibited (Figure S3d), without visible ventricular septal defect. The survival curve of *Nphp1*$^{+/+}$ or *Nphp1*$^{del2\text{-}20/del2\text{-}20}$ mice was exhibited (Figure S3e). The overall experiment was terminated at 72 weeks old of mice. No mice died beyond our setting experiment timepoints (5, 12, 36, and 72 weeks).

Discussion

Here we report for the first time, a *Nphp1* model which exhibits the characteristic renal phenotype of NPH consisting of corticomedullary cysts, dilated tubules, thickened tubular basement membranes and tubulointerstitial fibrosis (TIF), features absent in previous mouse models targeting exon 4 or 20 (12,13). The SH3 domain encoded by exon 5-6 of *Nphp1* has been reported to interact with the proline-rich motif of polycystin-1, thereby regulating the apoptotic response in mammals (25). In a genetic and biochemical network of known cystoproteins, polycystin-1 plays a central role in cystogenesis (26). For this reason, we speculated that the biochemical interaction between nephrocystin-1 and polycystin-1 underlying apoptotic response might contribute to the cystic phenotype of NPH. Given that the SH3 domain has a likely major functional role, the loss of function of this domain was identified as a prerequisite for gene inactivation. Our strategy was therefore to delete almost the entire *Nphp1* sequence apart from exon 1 to generate a complete loss of function allele.

Affected individuals with *NPHP1* mutations usually develop chronic kidney

disease (CKD) at a very young age (infantile, juvenile or adolescent stage), with conspicuous TIF (3), whereas TIF is highly correlated with CKD progression (27). In our study, fibrotic changes were initiated, demonstrated by elevated expression of FSP-1 and α-SMA in 12-week-old *Nphp1*$^{del2\text{-}20/del2\text{-}20}$ mice and by histology in 36 or 72-week-old *Nphp1*$^{del2\text{-}20/del2\text{-}20}$ mice kidneys. Impaired tubular urine concentrating capacity was also observed early at 8 weeks. However, owing to the indolent course of TIF and glomerulosclerosis, renal insufficiency was not prominent until 72 weeks in this recessive model. This unexpected slowly progressive disease pattern may be due to several reasons. First, there is 91% similarity and 83% identity between the human and mouse amino acid sequences of nephrocystin-1 (15). These small sequence differences could account for the discrepant phenotypes between human and mouse. On the other hand, a recent paper which included 5606 patients with adult-onset ESRD unexpectedly found a 0.5% (26 patients) prevalence of homozygous *NPHP1* whole gene deletions in this population (28). These data imply that some adult patients with *NPHP1* deficiency may present with slowly progressive CKD, consistent with our mouse model. The known role of different genetic backgrounds in modifying disease severity in our model deserves further study.

In our model, unlike diffuse inflammation infiltration observed in NPH patients, only focal infiltration could be detected, which mainly distributed around the affected glomerulus. Mononuclear phagocyte system appears to be one of the key components involving in the inflammatory network in chronic kidney diseases, including NPH (29,30,31). Nevertheless, there exist significant differences between mice and humans

in the mononuclear phagocyte system. It was not as similarly as expected when human and murine macrophages were aligned in response to a similar range of stimuli (32,33). Due to the divergent macrophage responses between these two species, the inflammation phenotypes could be incompletely accordant.

The overlap between the retinal phenotypes observed in previous *Nphp1* models and in our model emphasizes the role of this gene in retinal development (34). The RCC1-like domain (RLD) of Retinitis pigmentosa GTPase regulator (RPGR), a cilia-centrosomal protein frequently mutated in X-linked retinal degeneration and associated disorders, was found to bind to nephrocystin-1 (35). RPGR-containing multiprotein complexes play a key role in facilitating photoreceptor protein trafficking (36), which is involved in phototransduction and outer segment renewal (37,38,39). The disruption of the RPGR-NPHP1 complex owing to *Nphp1* mutation might result in loss of OS, IS, OPL and part of INL. As mentioned above, we observed low efficiency of AAV-OE rescue in retina. The pathogenesis of retinal involvement includes both developmental defects (dysplasia) and defects of tissue maintenance (degeneration) (40). Our treatment with AAV-OE in 5-week-old mice ameliorated the degeneration of retina to some extent but the dysplasia of OS and IS which occurred before day 21 (41) was irreversible, indicating that there is a critical therapeutic window for gene therapy during development, depending on the tissue.

There is an exceptionally high expression of *Nphp1* in mouse testis (15), suggesting a possible role in spermatogenesis. In this study, we confirm the crucial role of *Nphp1* in mouse spermatogenesis. Whether this finding is also present in humans remains to

be determined. Two reasons could explain the difficulty in detecting *Nphp1* deficiency-induced abnormal spermatogenesis in man. First, *Nphp1* is ubiquitously expressed at a relatively low level in majority of human organs, including the testis (15). Thus, there is little correlation between tissue expression pattern and the clinical phenotype. More importantly, NPH patients manifest with ESRD at a median age of 13 years and ESRD-induced deterioration of both spermatogenesis and steroidogenesis has long been recognized (42). In this regard, a primary spermatogenesis defect in human NPH may have been missed. In a recent study, an aberrant pattern of *NPHP1* expression and localization was observed in spermatozoa obtained from 103 infertile men (43), findings that support an essential role of NPHP1 in spermatogenesis. Re-expression of *Nphp1* in *Nphp1*$^{del2\text{-}20/del2\text{-}20}$ adult testis could not rescue this defect. This could be due to the impermeable blood-testis barrier (44), but remains an unsolved issue so far which includes all heritable diseases with testicular involvement. Gene transfer *in utero* may allow the targeting of expanding stem cell populations which become inaccessible later in life (45,46).

There were no gross skeletal or cardiac defects in our *Nphp1*$^{del2\text{-}20/del2\text{-}20}$ mice although there have been rare reports in previous studies of *Nphp1* deficiency (47). However, it should be noted that skeletal defects are more usually correlated with NPH patients with *Nphp12* or *Nphp13* mutations (48,49,50,51) and cardiac defects with mutations in *Nphp2* and *Nphp3* (52,53). In addition, modifier genes may modulate these phenotypes in NPH patients (47): the highly inbred genetic background in our mice could have suppressed any low penetrant traits.

We were unable to determine whether the measurable AAV-OE effect was still present in 72-week-old mice since this part of the study was terminated at 36 weeks. Nevertheless, the improvement in tubulointerstitial fibrosis (TIF) observed in 36-week-old *Nphp1*$^{del2\text{-}20/del2\text{-}20}$ mice after AAV-OE treatment suggests that a beneficial effect on kidney function would have been observed at the later time point. Future studies will examine if the early beneficial effect of AAV-OE treatment is sustained at 72 weeks and beyond.

In conclusion, we have generated a *Nphp1* model which faithfully reproduced the human NPH renal and retinal phenotypes while revealing a role in spermatogenesis. AAV-mediated gene therapy was successful in partially rescuing the kidney and retinal phenotypes. Since homozygous mutation of many cilia-associated genes are embryonically lethal in murine models (54,55,56), available ciliopathy models are rare. This *Nphp1* mouse will be valuable in revealing NPH phenotypes, clarifying common functions related to NPH and cilia genes, and providing a tractable model for drug development.

Materials and methods

Mice care and treatment

C57BL/6J mice were housed at the animal facility of Nanfang Hospital Southern Medical University on a 12 h/12 h light/dark cycle at 21°C and 50–55% humidity under specific pathogen-free (SPF) conditions with food and water available ad libitum. All animal experiments were performed based on ARRIVE1 guidelines (57)

and protocols approved by the Institutional Animal Care and Use Committee of Nanfang Hospital Southern Medical University. For *in vivo Nphp1* re-expression, type 9 adeno-associated viruses (AAV9) carrying recombinant *Nphp1-cDNA* plasmids (OE) or control plasmids (Vec) (Jikai Biology; Shanghai, China) were injected into the tail vein of 5-week-old C57BL/6J mice with a titer of 6×10^{10} copies for each animal. Individual weights were taken on all mice once a week until sacrifice. Body length was determined by measuring the nasal-to-anal distance. Tibia length was determined by measuring the knee-to-ankle distance. Mice were anesthetized by 3% pentobarbital sodium and sacrificed at 5, 12, 36 or 72 weeks of age.

Urine collection and analysis

For urine collection and analysis, mice were housed in the metabolic cages with free access to water and food for 24 hours. Body weight, water intake as well as urine output were monitored. Urine samples were centrifuged at 1,000 g at 4 ℃ for 5 min and the supernatants were saved for use. Urine specific gravity was measured using a refractometer according to the manufacturer's instructions (LOHAND BIOLOGICAL , LH-Y12, China).

Generation and Characterization of *Nphp1*$^{del2\text{-}20/del2\text{-}20}$ mice

To generate the *Nphp1*-knockout mice, four single-stranded oligos targeting upstream regions of exon 2 or downstream regions of exon 20 were designed using an online CRISPR tool (Table S1a, http://crispor.tefor.net/crispor.py). 10 putative

off-target sites of each sgRNA were listed (Table S1c). *Nphp1* sgRNAs and Cas9 mRNAs were microinjected into the pronuclei of mouse zygotes as described (58,59). Successfully injected C57BL/6J zygotes were surgically implanted into pseudo-pregnant recipient female mice. Potential founders were identified by PCR using the primers listed in Table S1d and Sanger sequencing (Table S1b). Based on the detected mutations, founder animals with two monoallelic deletions of 6bp and 39 796 bp were identified (Table S1b, *Nphp1*-q) and backcrossed to WT C57BL/6J mice to obtain $Nphp1^{+/del2\text{-}20}$ mice. These heterozygous mice were inbred to generate $Nphp1^{del2\text{-}20/del2\text{-}20}$ mice and their $Nphp1^{+/+}$ littermates, which were used for further studies.

Measurements of urea and creatinine

Whole blood was collected through the retroorbital venous plexus and allowed to clot in an Eppendorf tube. Serum was then separated by centrifugation. Urea and creatinine were measured on a Cobas C311 autoanalyzer (Roche).

Quantitative polymerase chain reaction (qPCR) assays

Total RNAs from tissues were extracted with TRIzol reagent (TaKaRa) in accordance with the manufacturer's instructions. cDNAs were generated with PrimeScript RT-PCR Kit (TaKaRa). mRNA expression was analyzed using SYBR Premix Ex Taq (TaKaRa) with an Applied Biosystems QuantStudio 6 Flex Real-Time PCR System (Thermo; Ringoes, NJ, USA). GAPDH was used for normalization.

Quantitation of specific gene expression was calculated using the ΔΔCt method. Primers used were detailed as follows: GAPDH (5'-GGCTCATGACCACAGTCCAT-3' and 5'-TACTTGGCAGGTTTCTCCAGG-3'), Nphp1 (5'-AGGGCAGTGTTTTCCGTCAG-3' and 5'-CCAGCACGGGATGACTGATT-3'), FSP-1 (5'-TTCCAGAAGGTGATGAG-3' and 5'-TCATGGCAATGCAGGACAGGAAGA-3'), and α-SMA (5'-GAGGCACCACTGAACCCTAA-3' and 5'-CATCTCCAGAGTCCAGCACA-3').

Protein extraction and western blotting

Tissues were lysed with RIPA buffer containing a protease inhibitor cocktail and a phosphatase inhibitor cocktail (Beyotime, China). The quantified protein samples were separated by electrophoresis on an SDS-polyacrylamide gel before transferring onto polyvinylidene fluoride (PVDF, Millipore, Bedford, MA, USA) membranes. After the membranes were blocked with skim milk (BD Biosciences, 90002-594) for 1 h at room temperature, they were incubated with specific antibody, followed by the secondary antibody conjugated to horseradish peroxidase. Next, the signals of the membranes were detected by FDbio-Dura ECL (enhanced chemiluminescence) kit (Fudebio, FD8020, China) according to the manufacturer's instructions. The following primary antibodies were used: anti-NPHP1(1:1000, Sigma-Aldrich, SAB2104055), anti-GAPDH (1:1000, Fudebio, FD0063), anti-FSP-1(1:1000, Cell Signaling Technology, 13018) and anti-α-SMA (1:1000, Cell Signaling Technology,

19245).

Histopathology

Kidney, retina, testis, and heart specimens were collected and immediately fixed with 4% paraformaldehyde at 4°C overnight. They were then treated with alcohol series and xylene before embedding in low-melting paraffin. Sections (4 μm) were deparaffinized with xylene and rehydrated in a graded alcohol series. H&E (Solarbio, G1120, China), PAS (Solarbio, G1281, China) or Masson (Solarbio, G1340, China) staining were applied by using standard protocols according to the manufacturer's instruction. Images were taken with OLYMPUS DP22 microscope or NanoZoomer-SQ Digital slide scanner (Hamamatsu, C13210-01, Japan). The fibrosis score was calculated using five consecutively selected fields of the renal cortex and medulla at 100× magnification in the 72-week-old renal sections stained with Masson staining, and then analyzed with Image J.

Immunofluorescent Staining

For immunofluorescence and visualizing nephrocystin-1 re-expression in kidney tissues, tissue slides were first incubated with antibodies against nephrocystin-1 (1:200, Lifespan Biosciences, LS-C334864) at 4°C overnight, followed by incubation with Alexa Fluor® 594-conjugated secondary antibodies (1:200, Jackson ImmunoResearch, 111-585-144). Kidney tissues were also stained with DAPI. Tissue slides were observed using OLYMPUS DP22 microscope.

Transmission Electron Microscopy

For ultrastructural analysis, mice kidney tissues (1 mm^3 in size) were fixed with 2.5% glutaral at room temperature for 1 h and then at 4°C overnight. After fixation, the samples were rinsed three times in PBS for 10 min each time. The tissues were then processed for transmission electron microscopy (TEM) following standard procedures. Finally, ultrathin sections were examined with an electron microscope (Hitachi H-7500, Japan) operated at 60 kV.

Statistics

Experiments were repeated independently at least three times. Data are shown as mean ± standard deviation (SD). Student's t-test and one-way ANOVA test were performed for comparing differences. $P < 0.05$ was considered statistically significant. Statistical analysis was performed using GraphPad Prism 8.0.

Acknowledgments:

This work was supported by the National Natural Science Foundations of China (Grant No. 81670610, No. 81470913). This work has partially been supported Guangdong Natural Science Foundation (Grant No. 2020A1515010286).

Conflict of Interest Statement:

All the authors declared no competing interests.

References

1 Hildebrandt, F., Singh-Sawhney, I., Schnieders, B., Centofante, L., Omran, H., Pohlmann, A., Schmaltz, C., Wedekind, H., Schubotz, C., Antignac, C. *et al.* (1993) Mapping of a gene for familial juvenile nephronophthisis: refining the map and defining flanking markers on chromosome 2. APN Study Group. *Am. J. Hum. Genet.*, **53**, 1256-1261.

2 Hamiwka, L.A., Midgley, J.P., Wade, A.W., Martz, K.L. and Grisaru, S. (2008) Outcomes of kidney transplantation in children with nephronophthisis: an analysis of the North American Pediatric Renal Trials and Collaborative Studies (NAPRTCS) Registry. *Pediatr. Transplant.*, **12**, 878-882.

3 Hildebrandt, F., Attanasio, M. and Otto, E. (2009) Nephronophthisis: disease mechanisms of a ciliopathy. *J. Am. Soc. Nephrol.*, **20**, 23-35.

4 Scolari, F., Viola, B.F., Ghiggeri, G.M., Caridi, G., Amoroso, A., Rampoldi, L. and Casari, G. (2003) Towards the identification of (a) gene(s) for autosomal dominant medullary cystic kidney disease. *J Nephrol*, **16**, 321-328.

5 Tang, X., Liu, C., Liu, X., Chen, J., Fan, X., Liu, J., Ma, D., Cao, G., Chen, Z., Xu, D. *et al.* (2020) Phenotype and genotype spectra of a Chinese cohort with nephronophthisis-related ciliopathy. *J. Med. Genet.*, in press.

6 Konig, J., Kranz, B., Konig, S., Schlingmann, K.P., Titieni, A., Tonshoff, B., Habbig, S., Pape, L., Haffner, K., Hansen, M. *et al.* (2017) Phenotypic Spectrum of Children with Nephronophthisis and Related Ciliopathies. *Clin. J. Am. Soc. Nephrol.*, **12**, 1974-1983.

7 Wolf, M.T. (2015) Nephronophthisis and related syndromes. *Curr. Opin. Pediatr.*, **27**, 201-211.

8 Macia, M.S., Halbritter, J., Delous, M., Bredrup, C., Gutter, A., Filhol, E., Mellgren, A.E.C., Leh, S., Bizet, A., Braun, D.A. *et al.* (2017) Mutations in MAPKBP1 Cause Juvenile or Late-Onset Cilia-Independent Nephronophthisis. *Am. J. Hum. Genet.*, **100**, 372.

9 Bizet, A.A., Becker-Heck, A., Ryan, R., Weber, K., Filhol, E., Krug, P., Halbritter, J., Delous, M., Lasbennes, M.C., Linghu, B. *et al.* (2015) Mutations in TRAF3IP1/IFT54 reveal a new role for IFT proteins in microtubule stabilization. *Nat Commun*, **6**, 8666.

10 Perrault, I., Saunier, S., Hanein, S., Filhol, E., Bizet, A.A., Collins, F., Salih, M.A., Gerber, S., Delphin, N., Bigot, K. *et al.* (2012) Mainzer-Saldino syndrome is a ciliopathy caused by IFT140 mutations. *Am. J. Hum. Genet.*, **90**, 864-870.

11 Fagerberg, L., Hallstrom, B.M., Oksvold, P., Kampf, C., Djureinovic, D., Odeberg, J., Habuka, M., Tahmasebpoor, S., Danielsson, A., Edlund, K. *et al.* (2014) Analysis of the Human Tissue-specific Expression by Genome-wide Integration of Transcriptomics and Antibody-based Proteomics. *Mol. Cell. Proteomics*, **13**, 397-406.

12 Jiang, S.T., Chiou, Y.Y., Wang, E., Lin, H.K., Lee, S.P., Lu, H.Y., Wang, C.K., Tang, M.J. and Li, H. (2008) Targeted disruption of Nphp1 causes male infertility due to defects in the later steps of sperm morphogenesis in mice. *Hum. Mol. Genet.*, **17**, 3368-3379.

13 Louie, C.M., Caridi, G., Lopes, V.S., Brancati, F., Kispert, A., Lancaster, M.A., Schlossman, A.M., Otto, E.A., Leitges, M., Grone, H.J. *et al.* (2010) AHI1 is required for photoreceptor outer segment development and is a modifier for retinal degeneration in nephronophthisis. *Nat. Genet.*, **42**, 175-180.

14 Kishimoto, K., Nomura, J., Ellegood, J., Fukumoto, K., Lerch, J.P., Moreno-De-Luca, D., Bourgeron, T., Tamada, K. and Takumi, T. (2017) Behavioral and neuroanatomical analyses in a genetic mouse model of 2q13 duplication. *Genes Cells*, **22**, 436-451.

15 Otto, E., Kispert, A., Schatzle, S., Lescher, B., Rensing, C. and Hildebrandt, F. (2000) Nephrocystin: gene expression and sequence conservation between human, mouse, and Caenorhabditis elegans. *J. Am. Soc. Nephrol.*, **11**, 270-282.

16 Hildebrandt, F., Otto, E., Rensing, C., Nothwang, H.G., Vollmer, M., Adolphs, J., Hanusch, H. and Brandis, M. (1997) A novel gene encoding an SH3 domain protein is mutated in nephronophthisis type 1. *Nat. Genet.*, **17**, 149-153.

17 Saunier, S., Calado, J., Heilig, R., Silbermann, F., Benessy, F., Morin, G., Konrad, M., Broyer, M., Gubler, M.C., Weissenbach, J. *et al.* (1997) A novel gene that encodes a protein with a putative src homology 3 domain is a candidate gene for familial juvenile nephronophthisis. *Hum. Mol. Genet.*, **6**, 2317-2323.

18 Donaldson, J.C., Dise, R.S., Ritchie, M.D. and Hanks, S.K. (2002) Nephrocystin-conserved domains involved in targeting to epithelial cell-cell junctions, interaction with filamins, and establishing cell polarity. *J. Biol. Chem.*, **277**, 29028-29035.

19 Konrad, M., Saunier, S., Heidet, L., Silbermann, F., Benessy, F., Calado, J., Le Paslier, D., Broyer, M., Gubler, M.C. and Antignac, C. (1996) Large homozygous deletions of the 2q13 region are a major cause of juvenile nephronophthisis. *Hum. Mol. Genet.*, **5**, 367-371.

20 Blowey, D.L., Querfeld, U., Geary, D., Warady, B.A. and Alon, U. (1996) Ultrasound findings in juvenile nephronophthisis. *Pediatr. Nephrol.*, **10**, 22-24.

21 Ala-Mello, S., Jaaskelainen, J. and Koskimies, O. (1998) Familial juvenile nephronophthisis. An ultrasonographic follow-up of seven patients. *Acta Radiol.*, **39**, 84-89.

22 Yue, Z., Lin, H., Li, M., Wang, H., Liu, T., Hu, M., Chen, H., Tong, H. and Sun, L. (2020) Clinical and pathological features and varied mutational spectra of pathogenic genes in 55 Chinese patients with nephronophthisis. *Clin. Chim. Acta*, **506**, 136-144.

23 Braun, D.A. and Hildebrandt, F. (2017) Ciliopathies. *Cold Spring Harb. Perspect. Biol.*, **9**.

24 Bruneval, P., Rossert, J. and Bariety, J. (2005) Renewal of FSP1: a marker of fibrogenesis on human renal biopsies. *Kidney Int.*, **68**, 1366-1367.

25 Wodarczyk, C., Distefano, G., Rowe, I., Gaetani, M., Bricoli, B., Muorah, M., Spitaleri, A., Mannella, V., Ricchiuto, P., Pema, M. *et al.* (2010) Nephrocystin-1 forms a complex with polycystin-1 via a polyproline motif/SH3 domain interaction and regulates the apoptotic response in mammals. *PLoS One*, **5**, e12719.

26 Ong, A.C. and Harris, P.C. (2015) A polycystin-centric view of cyst formation and disease: the polycystins revisited. *Kidney Int.*, **88**, 699-710.

27 Bohle, A., Mackensen-Haen, S. and von Gise, H. (1987) Significance of tubulointerstitial changes in the renal cortex for the excretory function and concentration ability of the kidney: a morphometric contribution. *Am. J. Nephrol.*, **7**, 421-433.

28 Snoek, R., van Setten, J., Keating, B.J., Israni, A.K., Jacobson, P.A., Oetting, W.S., Matas, A.J., Mannon, R.B., Zhang, Z., Zhang, W. *et al.* (2018) NPHP1 (Nephrocystin-1) Gene Deletions Cause Adult-Onset ESRD. *J. Am. Soc. Nephrol.*, **29**, 1772-1779.

29 Avesani, C.M., Carrero, J.J., Axelsson, J., Qureshi, A.R., Lindholm, B. and Stenvinkel, P. (2006) Inflammation and wasting in chronic kidney disease: Partners in crime. *Kidney Int.*, **70**, S8-S13.

30 Mihai, S., Codrici, E., Popescu, I.D., Enciu, A.M., Albulescu, L., Necula, L.G., Mambet, C., Anton, G. and Tanase, C. (2018) Inflammation-Related Mechanisms in Chronic Kidney Disease Prediction, Progression, and Outcome. *J Immunol Res*, **2018**, 2180373.

31 Viau, A., Bienaime, F., Lukas, K., Todkar, A.P., Knoll, M., Yakulov, T.A., Hofherr, A., Kretz, O., Helmstadter, M., Reichardt, W. *et al.* (2018) Cilia-localized LKB1 regulates chemokine signaling, macrophage recruitment, and tissue homeostasis in the kidney. *EMBO J.*, **37**.

32 Reynolds, G. and Haniffa, M. (2015) Human and Mouse Mononuclear Phagocyte Networks: A Tale of Two Species? *Front. Immunol.*, **6**.

33 Schroder, K., Irvine, K.M., Taylor, M.S., Bokil, N.J., Le Cao, K.A., Masterman, K.A., Labzin, L.I., Semple, C.A., Kapetanovic, R., Fairbairn, L. *et al.* (2012) Conservation and divergence in Toll-like receptor 4-regulated gene expression in primary human versus mouse macrophages. *Proc. Natl. Acad. Sci. U. S. A.*, **109**, E944-953.

34 Jiang, S.T., Chiou, Y.Y., Wang, E., Chien, Y.L., Ho, H.H., Tsai, F.J., Lin, C.Y., Tsai, S.P. and Li, H. (2009) Essential role of nephrocystin in photoreceptor intraflagellar transport in mouse. *Hum. Mol. Genet.*, **18**, 1566-1577.

35 Murga-Zamalloa, C.A., Desai, N.J., Hildebrandt, F. and Khanna, H. (2010) Interaction of ciliary disease protein retinitis pigmentosa GTPase regulator with nephronophthisis-associated proteins in mammalian retinas. *Mol. Vis.*, **16**, 1373-1381.

36 Patnaik, S.R., Raghupathy, R.K., Zhang, X., Mansfield, D. and Shu, X. (2015) The Role of RPGR and Its Interacting Proteins in Ciliopathies. *Journal of ophthalmology*, **2015**, 414781.

37 Kirschner, R., Rosenberg, T., Schultz-Heienbrok, R., Lenzner, S., Feil, S., Roepman, R., Cremers, F.P., Ropers, H.H. and Berger, W. (1999) RPGR transcription studies in mouse and human tissues reveal a retina-specific isoform that is disrupted in a patient with X-linked retinitis pigmentosa. *Hum. Mol. Genet.*, **8**, 1571-1578.

38 Young, R.W. and Droz, B. (1968) The renewal of protein in retinal rods and cones. *J. Cell Biol.*, **39**, 169-184.

39 Nair, K.S., Hanson, S.M., Kennedy, M.J., Hurley, J.B., Gurevich, V.V. and Slepak, V.Z. (2004) Direct binding of visual arrestin to microtubules determines the differential subcellular localization of its splice variants in rod photoreceptors. *J. Biol. Chem.*, **279**, 41240-41248.

40 Hildebrandt, F. and Zhou, W. (2007) Nephronophthisis-associated ciliopathies. *J. Am. Soc. Nephrol.*, **18**, 1855-1871.

41 LaVail, M.M. (1973) Kinetics of rod outer segment renewal in the developing mouse retina. *J. Cell Biol.*, **58**, 650-661.

42 Palmer, B.F. (2003) Sexual dysfunction in men and women with chronic kidney disease and end-stage kidney disease. *Adv. Ren. Replace. Ther.*, **10**, 48-60.

43 Devi, A.N., Anil Kumar, T.R., Pillai, S.M., Jayakrishnan, K. and Kumar, P.G. (2015) Expression profiles of NPHP1 in the germ cells in the semen of men with male factor infertility. *Andrology*, **3**, 685-693.

44 Kojima, Y., Hayashi, Y., Kurokawa, S., Mizuno, K., Sasaki, S. and Kohri, K. (2008) No evidence of germ-line transmission by adenovirus-mediated gene transfer to mouse testes. *Fertil. Steril.*, **89**, 1448-1454.

45 Schneider, H. and Coutelle, C. (1999) In utero gene therapy: the case for. *Nat. Med.*, **5**, 256-257.

46 Zanjani, E.D. and Anderson, W.F. (1999) Prospects for in utero human gene therapy. *Science*, **285**, 2084-2088.

47 Wolf, M.T. and Hildebrandt, F. (2011) Nephronophthisis. *Pediatr. Nephrol.*, **26**, 181-194.

48 Ellis, D.S., Heckenlively, J.R., Martin, C.L., Lachman, R.S., Sakati, N.A. and Rimoin, D.L. (1984) Leber's congenital amaurosis associated with familial juvenile nephronophthisis and cone-shaped epiphyses of the hands (the Saldino-Mainzer syndrome). *Am. J. Ophthalmol.*, **97**, 233-239.

49 Ryan, R., Failler, M., Reilly, M.L., Garfa-Traore, M., Delous, M., Filhol, E., Reboul, T., Bole-Feysot, C., Nitschke, P., Baudouin, V. *et al.* (2018) Functional characterization of tektin-1 in motile cilia and evidence for TEKT1 as a new candidate gene for motile ciliopathies. *Hum. Mol. Genet.*, **27**, 266-282.

50 Donaldson, M.D., Warner, A.A., Trompeter, R.S., Haycock, G.B. and Chantler, C. (1985) Familial juvenile nephronophthisis, Jeune's syndrome, and associated disorders. *Arch. Dis. Child.*, **60**, 426-434.

51 Moudgil, A., Bagga, A., Kamil, E.S., Rimoin, D.L., Lachman, R.S., Cohen, A.H. and Jordan, S.C. (1998)

Nephronophthisis associated with Ellis-van Creveld syndrome. *Pediatr. Nephrol.*, **12**, 20-22.

52 Bergmann, C., Fliegauf, M., Bruchle, N.O., Frank, V., Olbrich, H., Kirschner, J., Schermer, B., Schmedding, I., Kispert, A., Kranzlin, B. *et al.* (2008) Loss of nephrocystin-3 function can cause embryonic lethality, Meckel-Gruber-like syndrome, situs inversus, and renal-hepatic-pancreatic dysplasia. *Am. J. Hum. Genet.*, **82**, 959-970.

53 Otto, E.A., Schermer, B., Obara, T., O'Toole, J.F., Hiller, K.S., Mueller, A.M., Ruf, R.G., Hoefele, J., Beekmann, F., Landau, D. *et al.* (2003) Mutations in INVS encoding inversin cause nephronophthisis type 2, linking renal cystic disease to the function of primary cilia and left-right axis determination. *Nat. Genet.*, **34**, 413-420.

54 Windpassinger, C., Piard, J., Bonnard, C., Alfadhel, M., Lim, S., Bisteau, X., Blouin, S., Ali, N.B., Ng, A.Y.J., Lu, H. *et al.* (2017) CDK10 Mutations in Humans and Mice Cause Severe Growth Retardation, Spine Malformations, and Developmental Delays. *Am. J. Hum. Genet.*, **101**, 391-403.

55 Cabaud, O., Roubin, R., Comte, A., Bascunana, V., Serge, A., Sedjai, F., Birnbaum, D., Rosnet, O. and Acquaviva, C. (2018) Mutation of FOP/FGFR1OP in mice recapitulates human short rib-polydactyly ciliopathy. *Hum. Mol. Genet.*, **27**, 3377-3391.

56 Cheong, A., Degani, R., Tremblay, K.D. and Mager, J. (2019) A null allele of Dnaaf2 displays embryonic lethality and mimics human ciliary dyskinesia. *Hum. Mol. Genet.*, **28**, 2775-2784.

57 Kilkenny, C., Browne, W.J., Cuthill, I.C., Emerson, M. and Altman, D.G. (2010) Improving bioscience research reporting: the ARRIVE guidelines for reporting animal research. *PLoS Biol.*, **8**, e1000412.

58 Shao, Y., Guan, Y., Wang, L., Qiu, Z., Liu, M., Chen, Y., Wu, L., Li, Y., Ma, X., Liu, M. *et al.* (2014) CRISPR/Cas-mediated genome editing in the rat via direct injection of one-cell embryos. *Nat. Protoc.*, **9**, 2493-2512.

59 Ran, F.A., Hsu, P.D., Wright, J., Agarwala, V., Scott, D.A. and Zhang, F. (2013) Genome engineering using the CRISPR-Cas9 system. *Nat. Protoc.*, **8**, 2281-2308.

Figure Legend

Figure 1

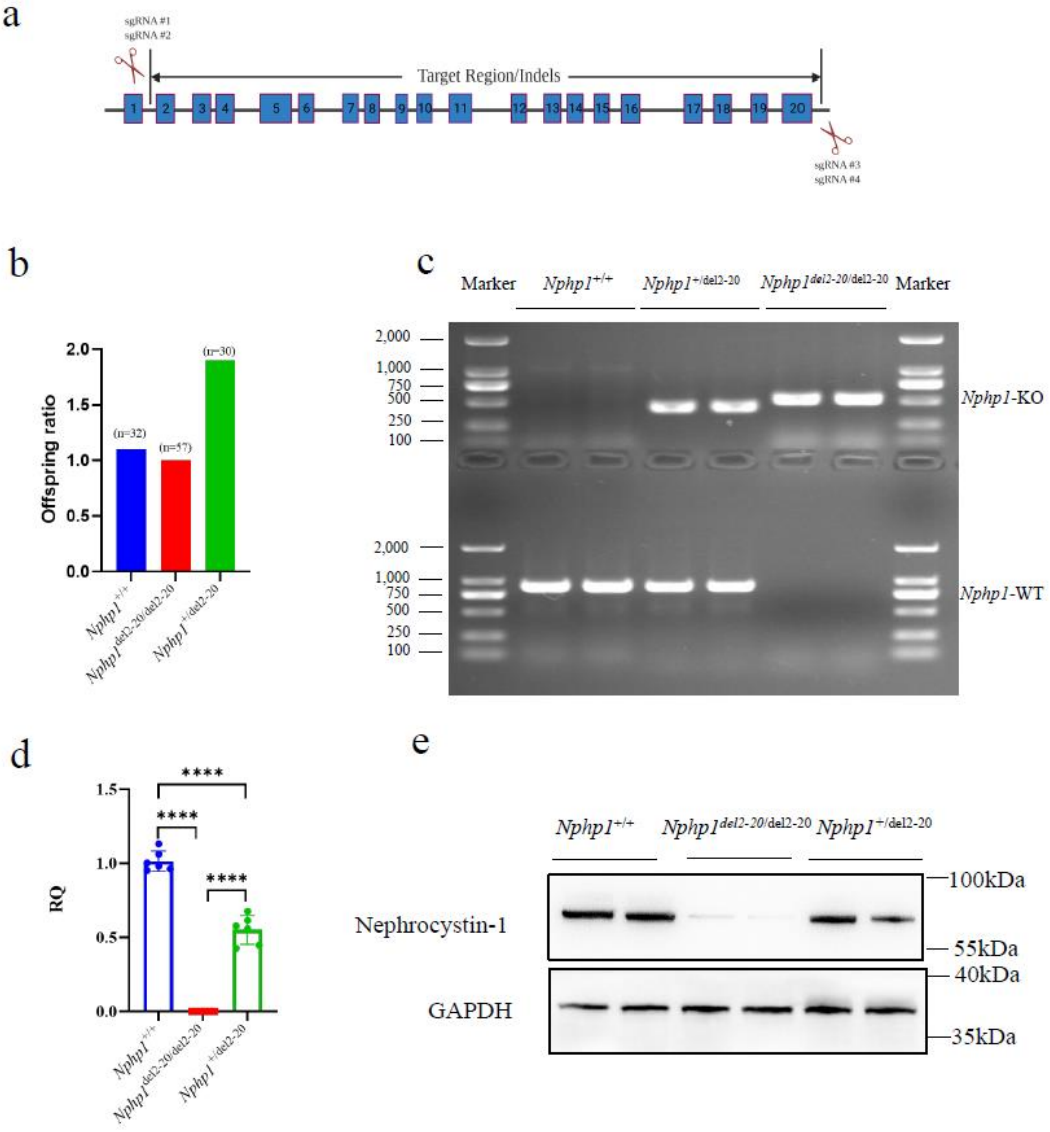

Figure 1. Generation and characterization of *Nphp1*$^{del2\text{-}20/del2\text{-}20}$ mice. a) Schematic of the CRISPR/Cas9 system-mediated inactivation of the *Nphp1* gene. In the *Nphp1*$^{del2\text{-}20/del2\text{-}20}$ strain allele, a fragment that encompasses exon 2-20 of *Nphp1* was deleted by using Cas 9 and sgRNA#1-4. sgRNA#1 and 2 target regions upstream exon 2 while sgRNA#3 and 4 target regions downstream exon 20. b) *Nphp1*$^{+/del2\text{-}20}$ mice (*Nphp1*-q) were intercrossed to produce pups that were weaned and genotyped at

2-3 weeks after birth. Total numbers of WT (*Nphp1*$^{+/+}$, n=32), homozygous (*Nphp1*$^{del2\text{-}20/del2\text{-}20}$, n=30), and heterozygous (*Nphp1*$^{+/del2\text{-}20}$, n=57) offspring were recorded, and the ratio of 3 genotypes was computed. c) PCR-based genotyping of *Nphp1*$^{+/+}$, *Nphp1*$^{+/del2\text{-}20}$, and *Nphp1*$^{del2\text{-}20/del2\text{-}20}$ mice. DNA was isolated from mouse tail biopsies and subjected to PCR analyses using the PCR primer pairs (*Nphp1*-WT-primer pair or *Nphp1*-KO-primer pair, as shown in Table S1d). d) Quantitative PCR analysis for *Nphp1* mRNA levels in *Nphp1*$^{+/+}$, *Nphp1*$^{del2\text{-}20/del2\text{-}20}$ or *Nphp1*$^{+/del2\text{-}20}$ kidneys (n=6 of each group). RQ, relative quantification. Data were normalized using glyceraldehyde-3-phosphate dehydrogenase (GAPDH) as a housekeeping gene. e) Western blot analysis for nephrocystin-1 and GAPDH protein levels in *Nphp1*$^{+/+}$, *Nphp1*$^{del2\text{-}20/del2\text{-}20}$ or *Nphp1*$^{+/del2\text{-}20}$ kidneys. Data or bar graphs represented the mean ± SD. * $P < 0.05$; ** $P < 0.01$; *** $P < 0.001$; **** $P < 0.0001$; ns, no significance.

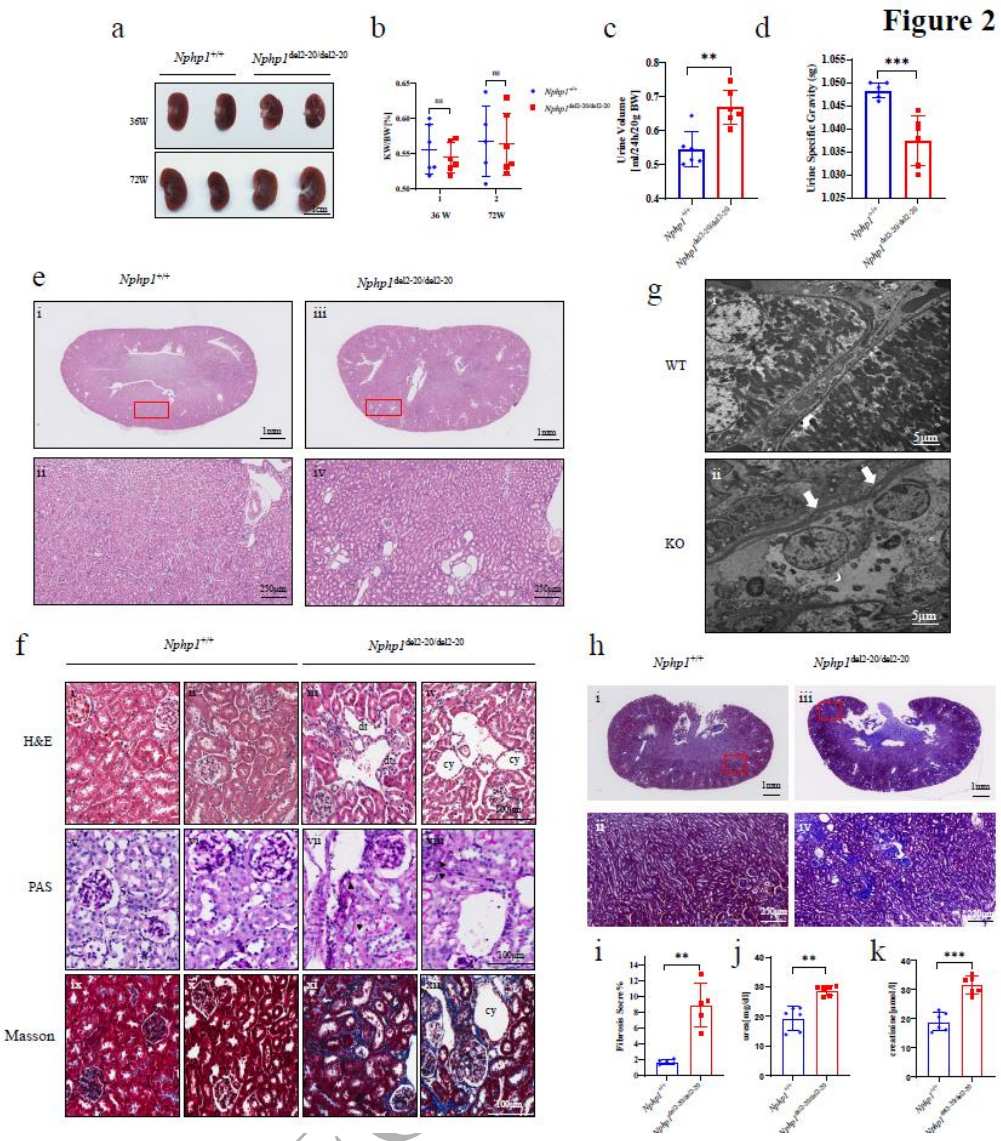

Figure 2. ***Nphp1*$^{del2\text{-}20/del2\text{-}20}$ mice recapitulate the renal phenotype of human NPH.**

a) Macroscopic pathology exhibited normal-sized kidneys of 36 and 72-week-old *Nphp1*$^{del2\text{-}20/del2\text{-}20}$ mice compared to those of *Nphp1*$^{+/+}$ mice (n=2 of each group). Scale bar=1cm. **b)** Kidney-to-body weight (KW/BW%) measurements of *Nphp1*$^{+/+}$ and *Nphp1*$^{del2\text{-}20/del2\text{-}20}$ mice at 36 and 72 weeks old(n=6 of each group), with no significant differences. **c)-d)** Analysis of voided 24-hour urine output (c) and urine specific gravity (sg, d) obtained from the 8-week-old *Nphp1*$^{+/+}$ (n=6) or *Nphp1*$^{del2\text{-}20/del2\text{-}20}$ mice (n=6). **e)** Hematoxylin and eosin (H&E) staining of renal

sections from 12-week-old mice. In *Nphp1*$^{del2\text{-}20/del2\text{-}20}$ mice kidney, there were multiple cysts of different sizes at the cortico-medullary junction (iii and iv). Boxed areas were magnified in ii and iv, respectively. Scale bar=1mm or 250μm. **f)** Hematoxylin and eosin (H&E, upper panel), Periodic acid–Schiff (PAS, middle panel), and Masson's trichrome (Masson, lower panel) staining of renal sections from 12 or 36-week-old mice (H&E for 12-week-old, PAS and Masson for 36-week-old mice). In comparison with *Nphp1*$^{+/+}$ mice, kidney sections from 12 or 36-week-old *Nphp1*$^{del2\text{-}20/del2\text{-}20}$ mice showed pronounced cyst formation (iv) and multiple dilated tubules (iii). Thickening tubular basement membrane (vii and viii) and tubulointerstitial fibrosis (xi and xii) could be seen in the renal sections from 36-week-old *Nphp1*$^{del2\text{-}20/del2\text{-}20}$ mice. Scale bar=100μm. **g)** Transmission electron microscopy (TEM) of kidneys from 36-week-old *Nphp1*$^{+/+}$ and *Nphp1*$^{del2\text{-}20/del2\text{-}20}$ mice. Thickening and layering tubular basement membrane could be observed in *Nphp1*$^{del2\text{-}20/del2\text{-}20}$ kidney (ii). Scale bar=5μm. **h)** Masson's trichrome (Masson) staining of renal sections from 72-week-old mice. Pronounced tubulointerstitial fibrosis was present in 72-week-old *Nphp1*$^{del2\text{-}20/del2\text{-}20}$ kidneys (iii and iv). Boxed areas were magnified in ii and iv, respectively. Scale bar=1mm or 250μm. **i)** Fibrosis score of *Nphp1*$^{+/+}$ or *Nphp1*$^{del2\text{-}20/del2\text{-}20}$ mice kidneys. n=6 of each group. **j)-k)** Analysis of serum urea (j) and creatinine (k) obtained from the 72-week-old *Nphp1*$^{+/+}$ (n=6) or *Nphp1*$^{del2\text{-}20/del2\text{-}20}$ mice (n=6), with significant elevation in *Nphp1*$^{del2\text{-}20/del2\text{-}20}$ group. dt=dilated tubule, cy=cyst. Black arrow indicated thickening tubular basement membrane and white arrow indicated layering tubular basement membrane. Data or

bar graphs represented the mean ± SD. * $P < 0.05$; ** $P < 0.01$; *** $P < 0.001$; **** $P < 0.0001$; ns, no significance.

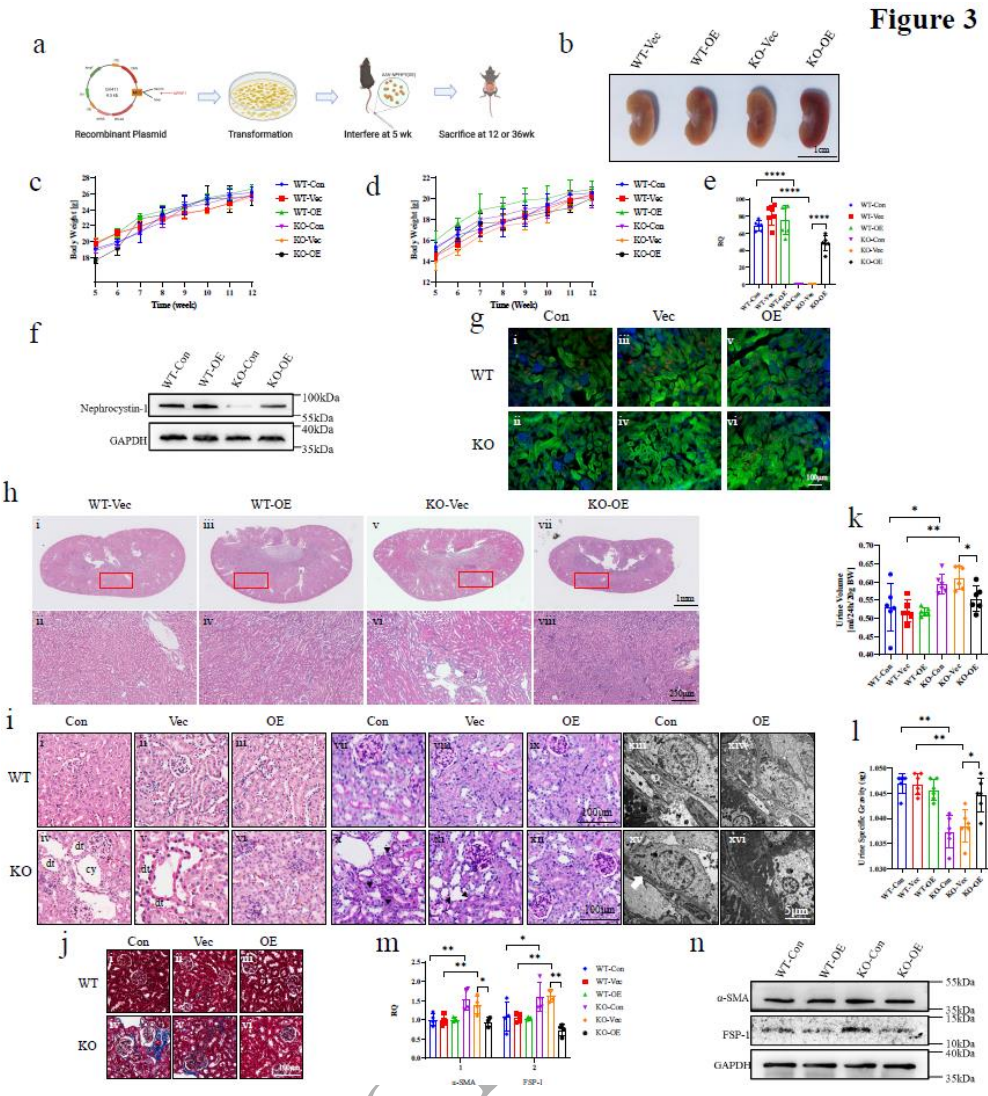

Figure 3. Re-expressing *Nphp1* in *Nphp1*$^{del2\text{-}20/del2\text{-}20}$ mice reversed cystic renal phenotype. a) Schematic representation of experiment timeline. Mice were treated by tail intravenous injection of recombinant adeno-associated virus serotype 9 (AAV9) containing either the murine *Nphp1* cDNA (OE) or empty vectors (Vec) 5 weeks (5 wk) after birth. Animals were then sacrificed at 12 or 36 weeks old. **b)** Gross appearance exhibited comparable-sized kidneys of 36 week-old *Nphp1*$^{del2\text{-}20/del2\text{-}20}$ mice with or without AAV9-OE treatment. Scale bar=1cm. **c)-d)** Body weight monitoring from interference day (5w) to sacrificing day (12w) in male **(c)** and female **(d)** AAV9-OE treated *Nphp1*$^{del2\text{-}20/del2\text{-}20}$ mice or *Nphp1*$^{+/+}$ mice, as well as their

matched controls. No significant body weight loss or gain was discovered. n=6 of each group. **e)** The mRNA levels of *Nphp1* in kidney tissues 7 weeks after AAV-OE treatment were determined by quantitative PCR assays and confirmed the re-expression of *Nphp1* in *Nphp1*$^{del2\text{-}20/del2\text{-}20}$ mice. n=6 of each group. RQ, relative quantification. Data were normalized using glyceraldehyde-3-phosphate dehydrogenase (GAPDH) as a housekeeping gene. **f)** Western blotting showed *Nphp1* re-expression in the kidney of 12-week-old *Nphp1*$^{del2\text{-}20/del2\text{-}20}$ mice injected with AAV-OE, using GAPDH as a housekeeping gene. **g)** Representative images of immunofluorescent staining (IF) of nephrocystin-1 in wild-type and knockout mice with or without AAV-OE treatment, indicating a successful re-expression of nephrocystin-1 (orange red) in AAV-OE treated KO mice. Using innate autofluorescence excited by 490-nm light, the renal tubule structures (green) could be approximately observed. It also demonstrated that nephrocystin-1 was mainly distributed at the apical surface of tubules. Nuclei were stained with 4,6-diamidino-2-phenylindole (DAPI). Scale bar=100μm. **h)** Hematoxylin and eosin (H&E) staining of renal sections from 12-week-old mice. In AAV-OE treated KO mouse kidney, corticomedullary cysts were barely seen (vii and viii). Boxed areas were magnified in ii, iv, vi and viii, respectively. Scale bar=1mm or 250μm. **i)** Hematoxylin and eosin (H&E, left panel, i-vi), Periodic acid–Schiff (PAS, right panel, vii-xii) staining and transmission electron microscopy (TEM, right panel, xiii-xvi) of renal sections from mice injected with AAV-OE (H&E for 12-week-old, PAS and TEM for 36-week-old mice). Corticomedullary cysts were barely seen in AAV-OE

treated knockout mice (vi). Thickness or layering of the tubular basement membranes (TBM) were improved (xii and xvi). Scale bar=100μm in H&E and PAS staining images. Scale=5μm in TEM images. **j)** Masson's trichrome (Masson) staining of renal sections from 36-week-old mice. Improved tubulointerstitial fibrosis was observed in 36-week-old *Nphp1*$^{del2\text{-}20/del2\text{-}20}$ kidneys with AAV-OE treatment (vi). Scale bar=100μm. **k)-l)** Analysis of voided 24-hour urine output (k) and urine specific gravity (l) obtained from the 8-week-old *Nphp1*$^{+/+}$ or *Nphp1*$^{del2\text{-}20/del2\text{-}20}$ mice with or without AAV-OE treatment. n=6 of each group. **m)-n)** The expression of FSP-1and α-SMA was measured by quantitative PCR **(m)** and western blotting assays **(n)**. FSP-1 and α-SMA were greatly or partly increased in *Nphp1*$^{del2\text{-}20/del2\text{-}20}$ background, respectively. This increase could be prevented by the treatment of AAV-OE. Data were normalized using glyceraldehyde-3-phosphate dehydrogenase (GAPDH) as a housekeeping gene. WT, *Nphp1*$^{+/+}$ mice; KO, *Nphp1*$^{del2\text{-}20/del2\text{-}20}$ mice. Con, without AAV treatment; Vec, with treatment of AAV9 containing empty vector; OE, with treatment of AAV9 containing murine *Nphp1* cDNA. dt=dilated tubule, cy=cyst. Black arrow indicated thickening tubular basement membrane and white arrow indicated layering tubular basement membrane. Data or bar graphs represented the mean ± SD. * $P < 0.05$; ** $P < 0.01$; *** $P < 0.001$; **** $P < 0.0001$; ns, no significance.

Figure 4

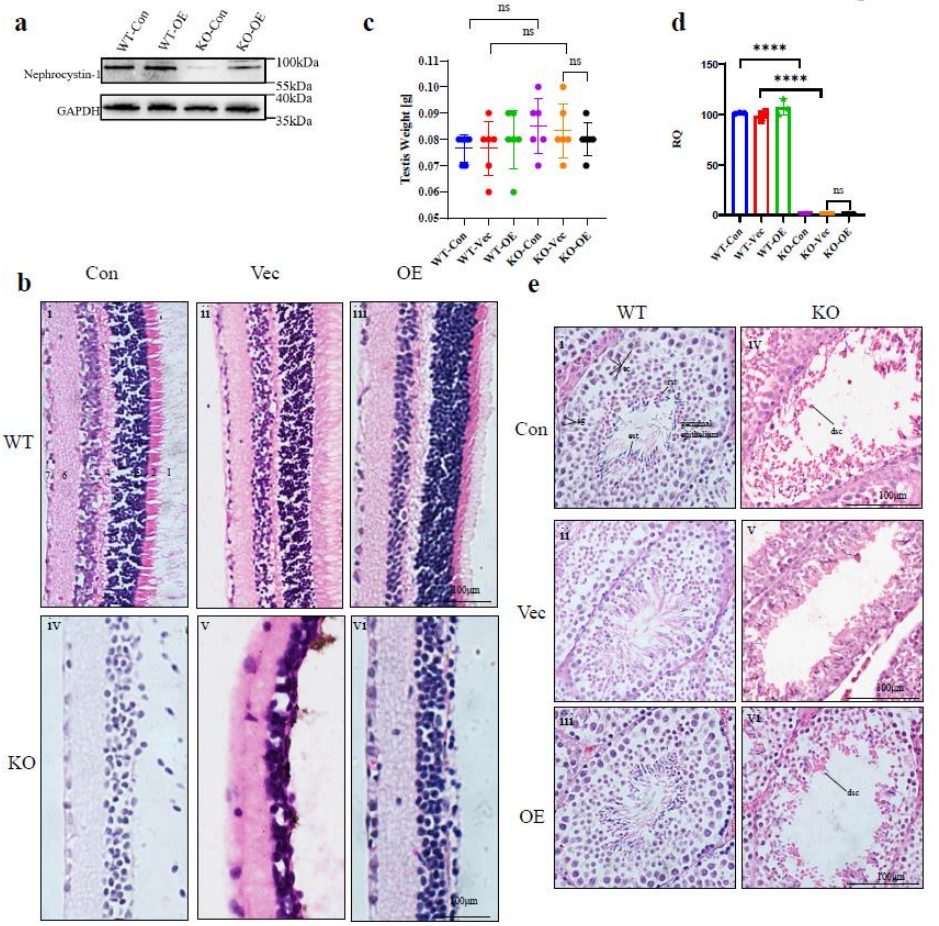

Figure 4. Deleting exon2-20 of *Nphp1* induces retinal degeneration and spermatogenic defects, which can be partially reversed by *Nphp1* re-expression. a) Western blotting showed *Nphp1* re-expression in the retina of *Nphp1*$^{del2\text{-}20/del2\text{-}20}$ mice injected with AAV-OE**,** normalized using GAPDH as a housekeeping gene. **b)** H&E staining of retinal sections from mice with or without AAV-OE treatment. The OS, IS, ONL, OPL, INL, IPL and GCL were all visible in the retina of 12-week-old *Nphp1*$^{+/+}$ mice (i). In the retina of *Nphp1*$^{del2\text{-}20/del2\text{-}20}$ mice, OS, IS and ONL were completely absent, with hardly existing OPL. The arrangement of INL was disorganized (iv). Increased number of nuclei and partially improved compactness were observed in

AAV-OE-treated *Nphp1*$^{del2\text{-}20/del2\text{-}20}$ mice (vi). 1, outer segment of the photoreceptors (OS); 2, inner segment of the photoreceptors (IS); 3, outer nuclear layer with photoreceptor cell nuclei (ONL); 4, outer plexiform layer (OPL); 5, inner nuclear layer (INL); 6, inner plexiform layer (IPL); 7, ganglion cell layer (GCL). Scale bar=100μm. **c)** No significant testis weight alterations were discovered in *Nphp1*$^{del2\text{-}20/del2\text{-}20}$ mice compared to those of *Nphp1*$^{+/+}$ mice or in AAV-OE-treated *Nphp1*$^{del2\text{-}20/del2\text{-}20}$ mice compared to those of their controls. n=6 of each group. **d)** The mRNA levels of *Nphp1* confirmed its failed re-expression in AAV-OE-treated *Nphp1*$^{del2\text{-}20/del2\text{-}20}$ testis. n=3 of each group. RQ, relative quantification. Data were normalized using glyceraldehyde-3-phosphate dehydrogenase (GAPDH) as a housekeeping gene. **e)** Representative images of H&E staining of testicular sections from *Nphp1*$^{del2\text{-}20/del2\text{-}20}$ mice with or without AAV-OE treatment. In *Nphp1*$^{+/+}$ mice, the well-bedded germinal epithelial was lined with different types of spermatogenic cells including sg, sc, rst, and est (i). In *Nphp1*$^{del2\text{-}20/del2\text{-}20}$ testis, the number of sg, sc, as well as rst produced during the spermatogenic process were prominently less than those of *Nphp1*$^{+/+}$ testis. Degenerated spermatogenic cells sloughed off into the lumen of seminiferous tubules. Est sporadically existed, with bizarre heads, and usually no or only rudimentary tails (iv). There was no overt improvement after AAV-OE treatment (vi). sg=spermatogonia, sc=spermatocytes, rst=round spermatids, est=elongated spermatids, dsc=degenerated bodies of spermatogenic cells. Scale bar=100μm. Data or bar graphs represented the mean ± SD. * $P < 0.05$; ** $P < 0.01$; *** $P < 0.001$; **** $P < 0.0001$; ns, no significance.

Abbreviations

NPH: Nephronophthisis

ESRD: End-stage renal disease

AAV9: Adenoviral-associated virus type 9

Mtln: T cell differentiation protein

Bub1: mitotic checkpoint serine/threonine kinase

SPF: specific pathogen-free

SD: standard deviation

sgRNAs: single guide RNAs

KO: knock out

FSP-1: Fibroblast-specific protein 1

α-SMA: α-smooth muscle actin

OS: outer segment of photoreceptors

IS: inner segment of photoreceptors

ONL: outer nuclear layer with photoreceptor cell nuclei

OPL: outer plexiform layer OPL

INL: inner nuclear layer

IPL: inner plexiform layer

GCL: ganglion cell layer

TIF: tubulointerstitial fibrosis

Supplementary Figure Legend:

Figure S1. *Nphp1*$^{del2\text{-}20/del2\text{-}20}$ mice recapitulate the renal phenotype of human NPH. a)-b) Analysis of serum urea (a) and creatinine (b) obtained from the 12-week-old *Nphp1*$^{+/+}$ (n=19) or *Nphp1*$^{del2\text{-}20/del2\text{-}20}$ mice (n=11). A non-significant but lower trend of serum urea and creatinine concentrations were shown in 12-week-old *Nphp1*$^{del2\text{-}20/del2\text{-}20}$ mice. **c)-d)** Analysis of voided 24-hour urine output (c) and urine specific gravity (sg, d) obtained from the 5-week-old *Nphp1*$^{+/+}$ (n=6) or *Nphp1*$^{del2\text{-}20/del2\text{-}20}$ mice (n=6). **e)** Masson's trichrome (Masson**)** staining of renal sections from 72-week-old mice. Poorer vascular patency and periglomerular fibrosis was present in 72-week-old *Nphp1*$^{del2\text{-}20/del2\text{-}20}$ mice (iii and iv) when compared to the control group (i and ii). Scale bar=50μm. **f)** Hematoxylin and eosin (H&E**)** staining of renal sections from 12-week-old mice in different lines. Similar renal phenotypes with cyst formation or tubule dilation could be observed in line *Nphp1-r* (ii) and *Nphp1-s* (iii). Scale bar=100μm. dt=dilated tubule, cy=cyst. Data or bar graphs represented the mean ± SD. * $P < 0.05$; ** $P < 0.01$; *** $P < 0.001$; **** $P < 0.0001$; ns, no significance.

Figure S2. Re-expressing *Nphp1* in *Nphp1*$^{del2\text{-}20/del2\text{-}20}$ mice reversed cystic renal phenotype. a) Masson's trichrome (Masson**)** staining of renal sections from 36-week-old mice. An improvement of vascular patency or periglomerular fibrosis after AAV-OE treatment in 36-week-old *Nphp1*$^{del2\text{-}20/del2\text{-}20}$ mice was observed (vi). Scale bar=50μm. **b)** Periodic acid–Schiff (PAS) staining of renal sections from 36-week-old

mice injected with AAV-OE. Ameliorated monocyte infiltration was observed after AAV-OE treatment (vi). Scale bar=100μm. **c)-d)** Analysis of serum urea (c) and creatinine (d) obtained from the 36-week-old mice, with or without AAV-OE treatment. No significance could be observed. n=6 of each group. Data or bar graphs represented the mean ± SD. * $P < 0.05$; ** $P < 0.01$; *** $P < 0.001$; **** $P < 0.0001$; ns, no significance.

Figure S3. Extrarenal phenotypes of *Nphp1*$^{del2\text{-}20/del2\text{-}20}$ mice. a)-b) Body length measurement in male (a) and female (b) mice of various ages. n=6 of each group. **c)** Tibia length measurement in 12-week-old *Nphp1*$^{+/+}$ or *Nphp1*$^{del2\text{-}20/del2\text{-}20}$ mice. n=6 of each group. **d)** Hematoxylin and eosin (H&E**)** staining of cardiac sections from 12-week-old *Nphp1*$^{+/+}$ or *Nphp1*$^{del2\text{-}20/del2\text{-}20}$ mice. No visible ventricular septal defect could be observed in *Nphp1*$^{del2\text{-}20/del2\text{-}20}$ mice. Scale bar=2.5mm. **e)** The survival curve of *Nphp1*$^{+/+}$ or *Nphp1*$^{del2\text{-}20/del2\text{-}20}$ mice. The overall experiment was terminated at 72 weeks old of mice. No mice died beyond our setting experiment timepoints (5, 12, 36, and 72 weeks). LV=left ventricle, VS=ventricular septum, RV=right ventricle. Data or bar graphs represented the mean ± SD. * $P < 0.05$; ** $P < 0.01$; *** $P < 0.001$; **** $P < 0.0001$; ns, no significance.

Figure S1

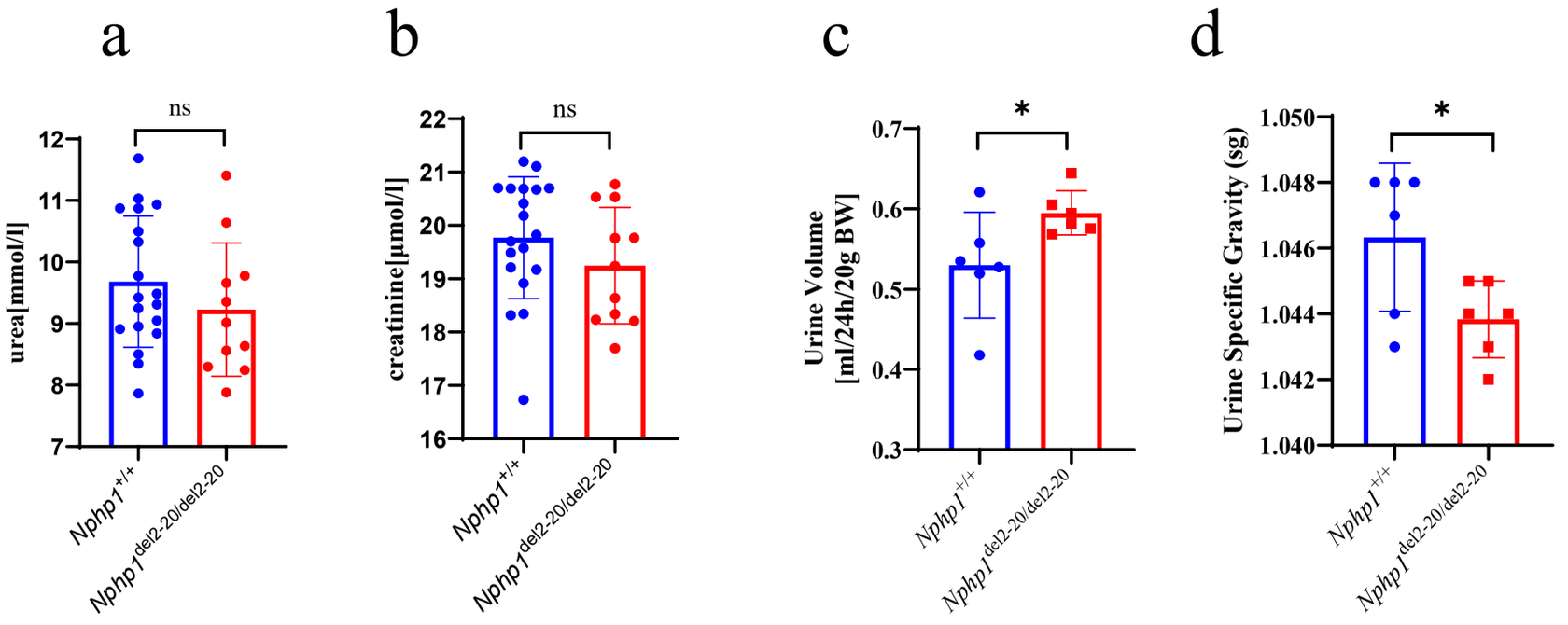
a
b
c
d
ns
ns
*
*
urea[mmol/l]
creatinine[μmol/l]
Urine Volume [ml/24h/20g BW]
Urine Specific Gravity (sg)
Nphp1+/+
Nphp1del2-20/del2-20

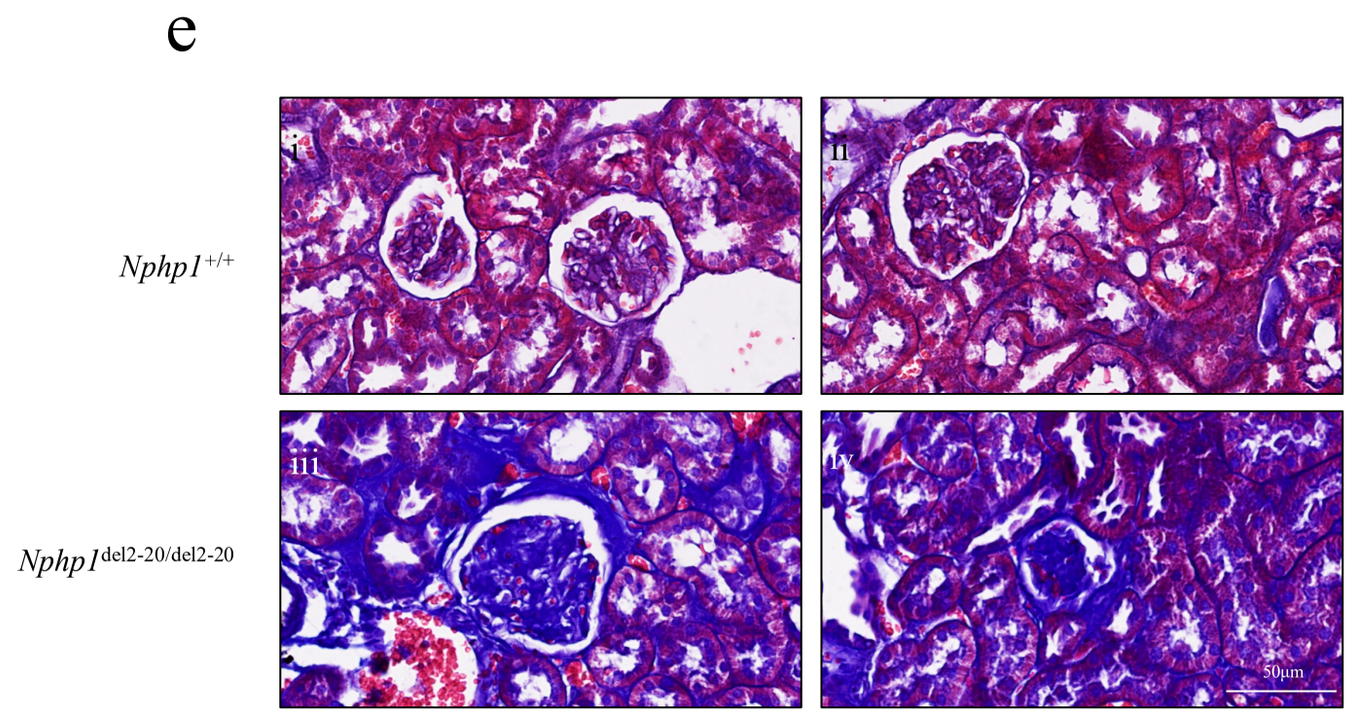
e
Nphp1+/+
Nphp1del2-20/del2-20
i
ii
iii
iv
50μm

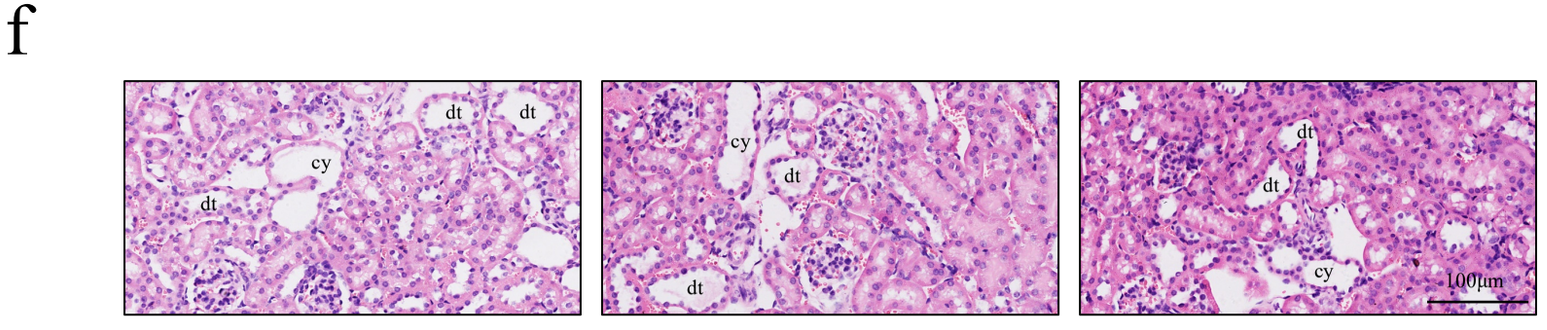
f
dt
cy
100μm
Nphp1-q
Nphp1-r
Nphp1-s

Figure S2

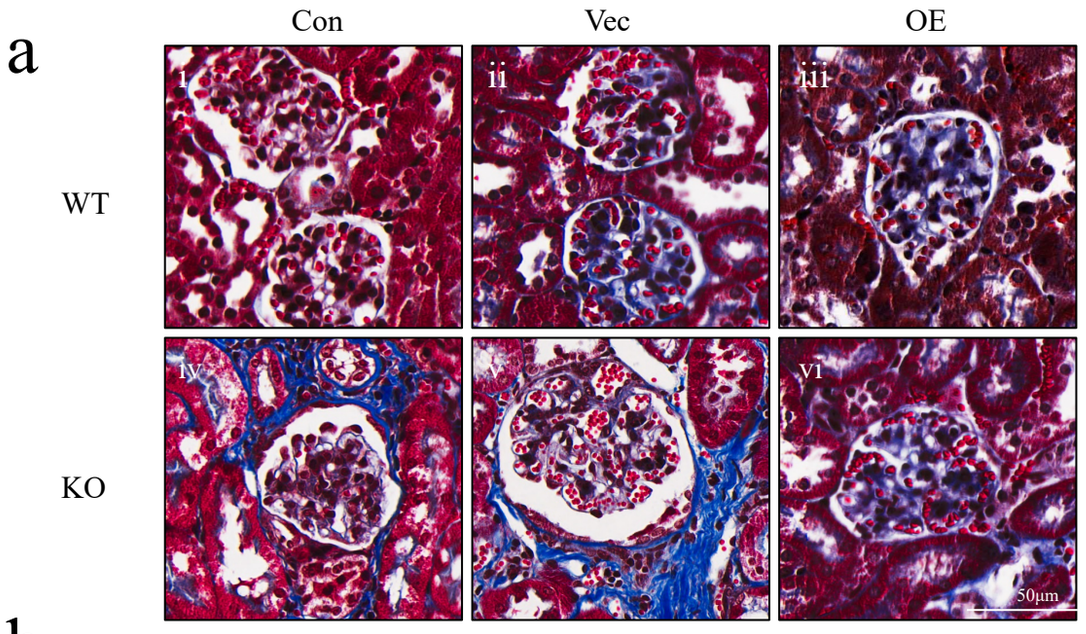
a
Con
Vec
OE
WT
KO
i
ii
iii
iv
v
vi
50μm

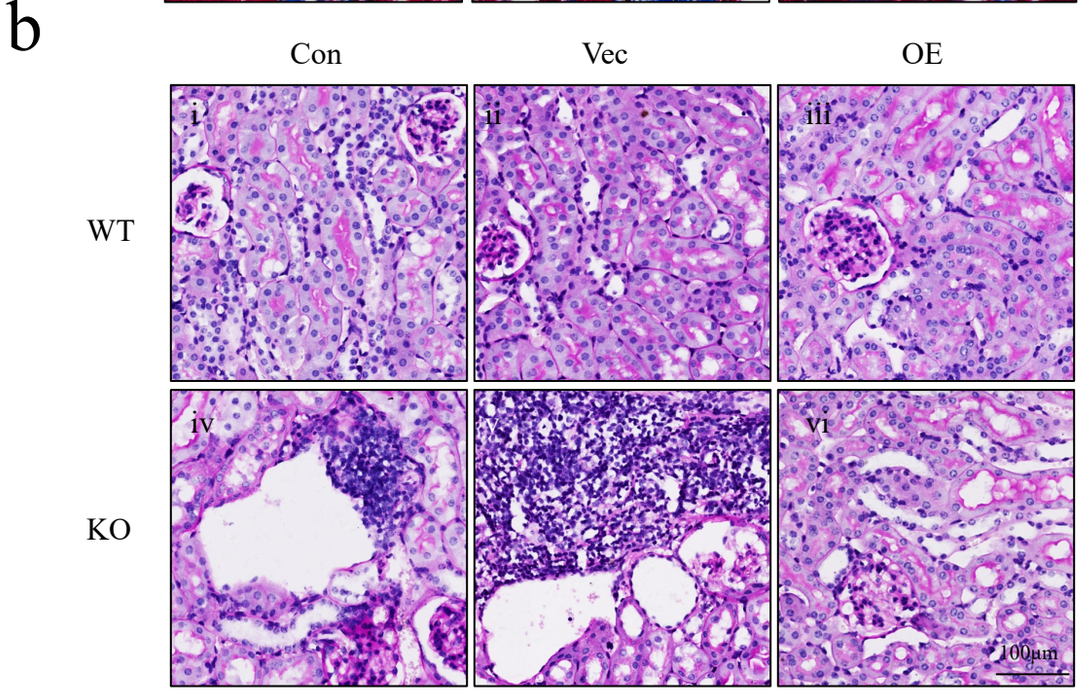
b
Con
Vec
OE
WT
KO
i
ii
iii
iv
v
vi
100μm

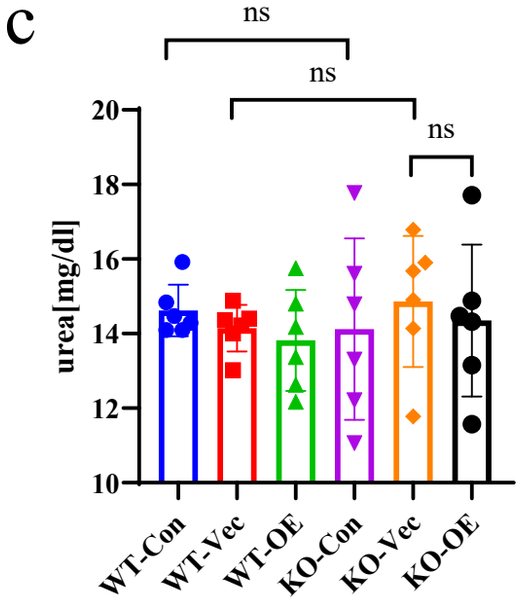
c
ns
ns
ns
urea[mg/dl]
20
18
16
14
12
10
WT-Con
WT-Vec
WT-OE
KO-Con
KO-Vec
KO-OE

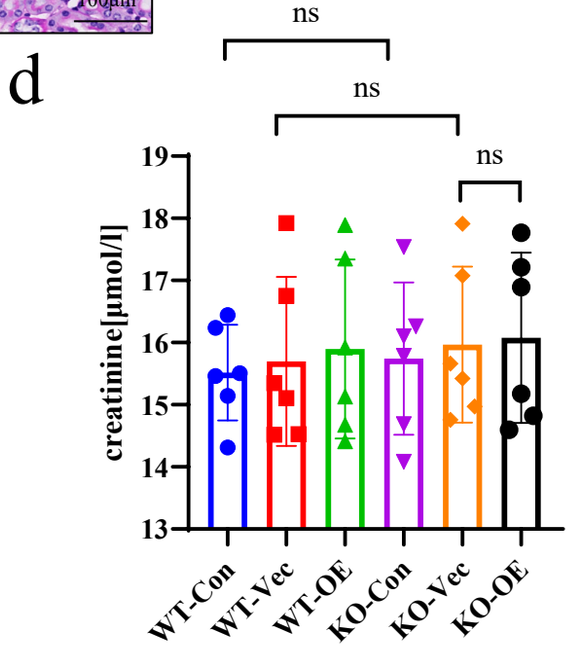
d
ns
ns
ns
creatinine[μmol/l]
19
18
17
16
15
14
13
WT-Con
WT-Vec
WT-OE
KO-Con
KO-Vec
KO-OE

Figure S3

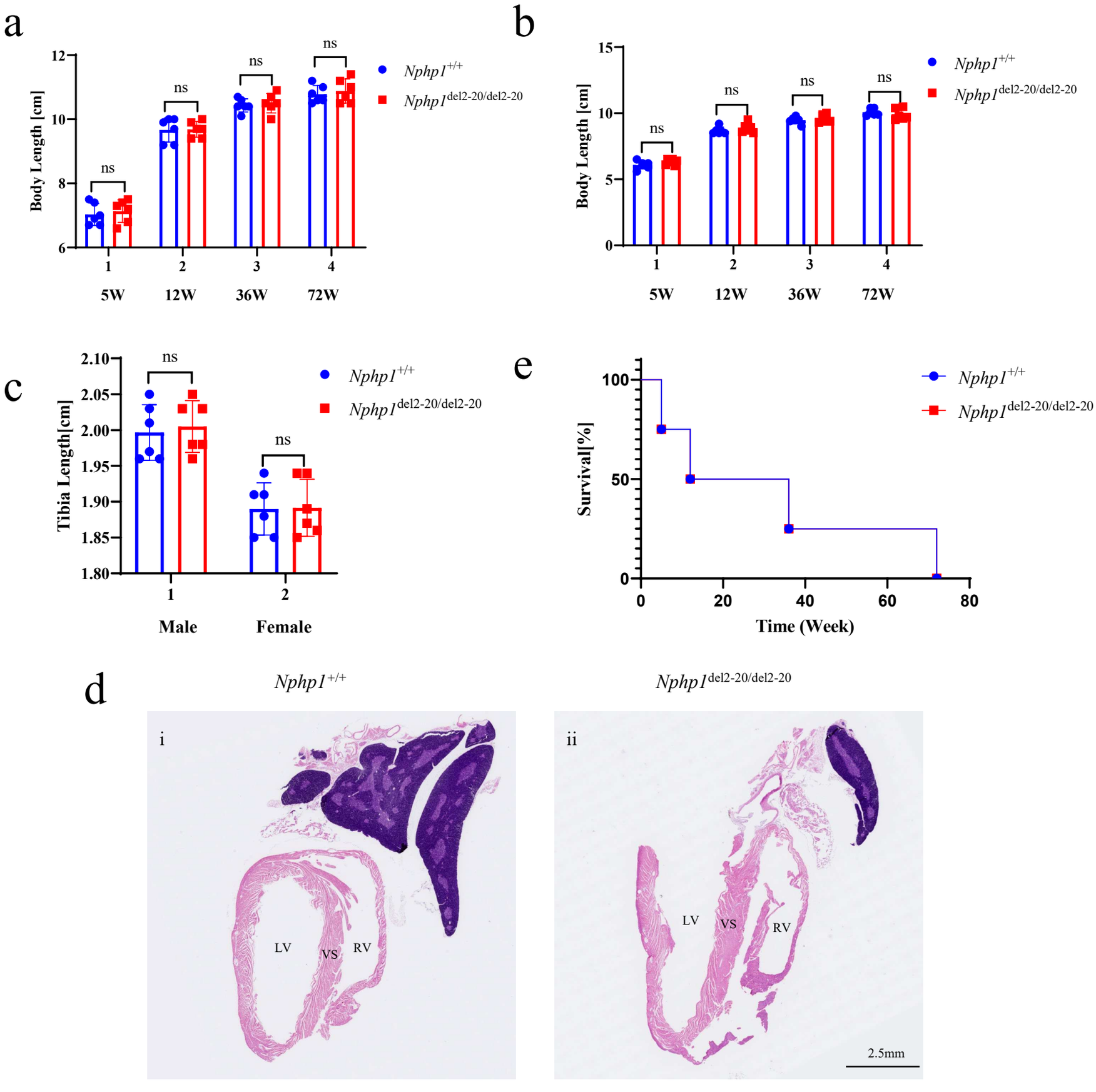
a
Body Length [cm]
12
10
8
6
ns
ns
ns
ns
1
2
3
4
5W
12W
36W
72W
Nphp1+/+
Nphp1del2-20/del2-20
b
Body Length [cm]
15
10
5
0
ns
ns
ns
ns
1
2
3
4
5W
12W
36W
72W
Nphp1+/+
Nphp1del2-20/del2-20
c
Tibia Length[cm]
2.10
2.05
2.00
1.95
1.90
1.85
1.80
ns
ns
1
2
Male
Female
Nphp1+/+
Nphp1del2-20/del2-20
e
Survival[%]
100
50
0
0
20
40
60
80
Time (Week)
Nphp1+/+
Nphp1del2-20/del2-20
d
Nphp1+/+
Nphp1del2-20/del2-20
i
ii
LV
VS
RV
LV
VS
RV
2.5mm

Supplementary Tables:

Table S1. Generation and characterization of *Nphp1*$^{del2-20/del2-20}$ mice.

Table S1a. Sequence of sgRNA targeting exon2-20 of *Nphp1*

sgRNA	Sequence (5' to 3')	PAM
sgRNA#1	AGGGTTGTACAGATGCACCT	GGG
sgRNA#2	CATTATAAGATGCTAATGGT	AGG
sgRNA#3	CTGATACAAATGTAATGCCA	AGG
sgRNA#4	GTGCTTGTCTAGTTCGTGCA	AGG

sgRNA=single guide RNA; PAM=protospacer adjacent motif.

Table S1b. *Nphp1* mutant mice generated by CRISPR/Cas9 using sgRNAs targeting exon 2-20

Mouse line	Indels
Nphp1-a	gcctcagggttgtacagatgcAacctgggaccttaaca//aaacaggcattataagat----- 39,753bp-----ACacagggctctgtggtagagtgctt-----5bp----- GCATGATGATGTGAATGGTATGATTTTTGTGATGTTTCCTATT TTTCGGATGTCTTGTTCGTCTGCCAGGCTATGAATGATTGAG CCAGAGCATATAAAGAGTATAGCTTTGAAGAATGCGTGGGT ACAGATGTGTAGGAATGCTAGGTGTGGTTGGTTTATTCCTA GCGTCACTATTATCAGGCCTAGTTGGCTTGATGTAGAGAAG GCAATGATTTTTTTGATGTCGTTTTGGGTGAGAGCACAAAT AGCTGTAAATAATGTGGTTAGGGCTCTGgcaaggccctgggttccaacc c
Nphp1-b	agtacagtaaacgtgcgcctcagggttgtacagat-----39,924bp----- gttccaaccccagcactgcaaaggcagtctaatat

Nphp1-c	cagtaaacgtgcgcctcagggttgtacagatgca-----39,912bp-----aggccctgggttccaaccccagcactgcaaaggc
Nphp1-d	cagggttgtacagatg-----11bp-----ttaacagagtgct//ataagatgctaa-----39,746bp-----ggacagggctctgtggtagagtgcttgtcta
Nphp1-e	agggttgtacagatgcAacctgggac//taagatgctaat-----39,781bp-----tgcaaggccctgggttccaaccccagcactgcaaaggc
Nphp1-f	gaatccgtctgttaaagtacag-----39,909bp-----ggctctgtggtagagtgcttgtctag-----6bp-----caaggccctgggttccaaccccagcactg
Nphp1-g	aacgtgcgcctcagggttgtacagatgcAacctgggaccttaa//ataagatgctaatg-----39,852bp-----ttgctaatgatatttgtaggttattcag
Nphp1-h	ttaaagtacagtaaacgtgcgcctcagg-----40,079bp-----gttagaacaaatgcagaattcttgtctt
Nphp1-i	aacgtgcgcctcagggttgtacagatgcAacctgggaccttaa//tataagatgctaat-----39,781bp-----tgcaaggccctgggttccaaccccagca
Nphp1-j	aaacgtgcgcctcagggttgtacagatg-----6bp-----ggaccttaacagag//acaggcattataag-----39,788bp-Tgtgcaaggccctgggttccaaccccagc
Nphp1-k	cgtgcgcctcagggttgtacagatgcac-----7bp-----cttaacagagtgct//tataagatgctaat-----39,781bp-----tgcaaggccctgggttccaaccccagca
Nphp1-l	aaaactcacttgtagtggaaaaaatgag-----40,067bp-----caaggccctgggttccaaccccagcact
Nphp1-m	cgtgcgcctcagggttgtacagatgcac-----39,868bp-----caaggacagggctctgtggtagagtgct
Nphp1-n	acgtgcgcctcagggttgtacagatgca-----39,908bp-----tgcaaggccctgggttccaaccccagca
Nphp1-o	gggaaaaactcacttgtagtggaaaaaatgagctg-----40,074bp-----ggttccaaccccagcactgcaaaggcagtctaata
Nphp1-p	agtgggaaaaactcacttgtagtggaaaaaatgag-----40,067bp-----

	caaggccctgggttccaaccccagcactgcaaagg
Nphp1-q	cagggttgtacagatg-----6bp-----
	ggaccttaacagagtgct//agataaacaggcattataa-----39,796bp-----
	gccctgggttccaaccccagcactg
Nphp1-r	aaacgtgcgcctcagggttgtacagatgca-----39,912bp-----
	aggccctgggttccaaccccagcactgcaa
Nphp1-s	gcgcctcagggttgtacagatgcac-----39,868bp-----
	caaggacagggctctgtggtagagtgcttgtctagttcgTtgcaaggccctgggttcc
Nphp1-t	cctcagggttgtacag-----11bp-----accttaacagagtgctct//aacaggcattataagatg-
	----39,943bp-----gttagaacaaatgcagaattctt

Indel=insertion/deletion mutation; *Nphp1-q* was selected to intercross and produce offspring.

Table S1c. Off-target sites of sgRNAs and relative Primers

sgRNA	Off-target Sequence	Forward Primer (5' to 3')	Reverse Primer (5' to 3')
sgRNA#1	AGGGCTATATAGATG AACCTTGG	GTCTCCTTAGTGTC TAACCACCATG	GATTTGGGAAGTC CAATCCTAACC
sgRNA#1	AGGGCTGCACAGAT GAAACTTGG	AGAATCTAAGGAGA GCTGCTCTGG	ACTCCTCCCTCTTC AGATGTCAG
sgRNA#1	AGGGTCTCACAGAT GAACCTTGG	TGCACTTGCTTGTG TCAACCAC	CAAGGGATTTAGC TCCTCACTG
sgRNA#1	CTGGTTATACAAATG CACCTCGG	CAAGCCATGCTTAT CCTATGCTG	GCTTCAGCCTACA CTTGCTATCTG
sgRNA#1	TGGGTTATGCAGAT GCACCACGG	GGCTTTGGGCTCAA GATGAAG	GCAGACTTGTGGG ACACACTTT
sgRNA#1	TGGGTTCCACAGAT GCAACTTGG	AGTCTGCTCTCTAC TCTGGAAGACTG	GGGATTTGGTACT GATTCACAGAG

sgRNA#1	AATGTAGTACAGAT	TAACTCCACAAGAG	CATCAATGTCCAA
	GAACCTGGG	GTGCCAAG	ACTAAGCACAG
sgRNA#1	AGGGCTGCCCAGAA	GTCATCTGTTCATGT	AAATCTAGGTGAG
	GCACCTTGG	CCAAGGTG	TCCAGCCTGTAG
sgRNA#1	AGGTTTGTAAAGAT	CCATTGACTGGCCA	CAATGATACATCC
	AAACCTGGG	AGTTTGTC	AGTATGGCAGC
sgRNA#1	AGGTTTGTAAAGAT	CATTGACTGGCCAA	GGCAATGATACAT
	AAACCTTGG	GTTTGTC	CCAGTATGGC
sgRNA#2	TAATGTAAGATGCTA	CAACTGGAAAGATG	CCAAACTCTCCTT
	ATGATAGG	GCAGTGATAG	TAGCCACTG
sgRNA#2	TATTGTAACATACTA	CAAAATGTTGCTGG	TTAGAATGTCACC
	ATGGTGGG	TGGTCTG	AGGCAGAGG
sgRNA#2	TATGAAAAGATGCT	CCCACTTGCTCGTG	ATCTATCAGAAGG
	AATGTTGGG	TAATGTCTC	CAGTCATCCC
sgRNA#2	GTTTATAAGATGTTA	AGGGAAGAGTAGC	CAATAGAACTGGG
	ATGTTTGG	AGCAGTCTTTG	CAGATGTCTTC
sgRNA#2	AAATATAAAATGCTA	AACTCCAGCTGTGT	CACAAAGGCATCT
	ATTGTGGG	CAAGTTGAC	AAGGCAAGTC
sgRNA#2	AAAAAAAAGATGCT	GCGTTCACTAGAAC	GAGACATAGCTCA
	AATGGTGGG	TTTGCTTAGC	TTGCTGTCACTC
sgRNA#2	AAATGTAAGATGCT	AGACCACTCCAAGA	TCATTCCTCAGTTC
	AATGGAGGG	ACTCTCCTG	GAGGGATC
sgRNA#2	CATTAAGAGTTGCT	CACTGTGATAGAGT	GCCAGAGGCATCA
	AAAGGTGGG	GCCCATGTTC	GAACTGTAGA
sgRNA#2	CTTTACAAGATGTA	CCTGTGCATGGTGT	CTCTGTTTGGACT
	AATGGTTGG	TAGGTACTAAC	AGAGGCAGAGTG
sgRNA#2	AAATATAAGATGCTG	TCTCAGGTCAGGCA	GCATGAGATACTT
	AAGGTGGG	ATAGCAAC	GGGTATCTGC
sgRNA#3	CAGATACAGTTATAA	TCACCAGGATGCAT	GAATTGCTAACCC

	TGCCATGG	AGGAACAG	TGCTTACAGG
sgRNA#3	CTGGTAAAATTGTA	ATAAGGCAGATCAG	GTTTCCACTAAGG
	AAGCCATGG	CCAAGGTC	TTTCCTTGCC
sgRNA#3	CAGACACAAATCCA	GAACGATTGCCTCA	ACATTCAAGGCAG
	ATGCCAAGG	AAGGTGAG	GATCACAGAC
sgRNA#3	ATGATATAAATATAA	GAGTAGTAGGCCAG	GCTTGTTCTGATTC
	TGCTATGG	AACATCATGG	AGACCAACTG
sgRNA#3	GAGATACAAATGAA	GGTCAGATCATGTT	CAGGAACAGGGA
	ATGTCAGGG	AGAGCCAGG	CTTTCTCAAC
sgRNA#3	ATGATACAAATTTAA	GTTACTGGACCAAG	CTCTAAATGTCCT
	AACCATGG	CCAAGACAG	GCTCCATGC
sgRNA#3	CTGACACAGAAGTA	CCAAGTAGAAATCG	CATACAGAAGACA
	ATGTCAAGG	CAGGTCATAG	CCTGAGCAGAC
sgRNA#3	GTGAAAAAAATATA	TTGTGAGTTGTGGC	TTTGATATGGGCAC
	ATGCCAAGG	TCCAATG	AGAGACCC
sgRNA#3	CTGTTGAAAATGTA	TCTTATGAGCCTGC	AGGAGGATGAGAC
	ATACCAGGG	CAGCATTC	ATGCTGTCTC
sgRNA#3	CAGGTACAGTTGTA	GCCAGGCTATAATG	AAGGCACTCACCA
	ATGCCATGG	CCTCTACAAG	CAGACAGCTT
sgRNA#4	GAGTTTGCCTAGTT	CAAAGTTTGCAGCA	CAACACGCATGGT
	CATGCAAGG	CAGGAGAC	CTCAAACAG
sgRNA#4	GTACTTGCCTAGCTC	TGAGGAGAAGGTTC	GCATGGGTAGCTG
	ATGCAAGG	TGGTTAGATC	TAATGAAGG
sgRNA#4	GTGCTTGCCTAGCT	TTGGGCGTATTTCC	CATGCGTTGGGCT
	CATACAAGG	CTCTGAG	CAGTATTG
sgRNA#4	GTGCTTGCCTAGCA	GGAAGGAAGGAGT	TGGAGAGAGGTAA
	CATGCAAGG	ATGTTCCATC	GCTGAAACAG
sgRNA#4	GTGCCTGCCTAGCA	TGGGCTCTGTGCTA	AGCTGTTGATGGA
	CGTGCAAGG	TTCCAAC	CCATGACAAC

sgRNA#4	GAGCTTGTCTAGCA	CACAAGTAGCTGCA	AACTGTCCACATG
	CATGCAAGG	ACTCCAGTTC	CTGACTTGC
sgRNA#4	GCATTTGTCTAGCTC	GGACGTGTTCACTT	TACTTTGGCGCAT
	GTGCAAGG	AGGAAAGGTC	CTGTGTCAG
sgRNA#4	GTGCTTGACTAGCA	TCTAGAGGACAACA	TTTCCGAGGAGAT
	CATGCAAGG	GTAGGGTATGG	GAAGGGATC
sgRNA#4	GAGCTTGTCTAGAA	GTGGAGCTAATGAC	ATATTCCACCCATT
	CATGCAGGG	AAGGAGCTG	CTGGGCTC
sgRNA#4	GTGCTTGGCTAGCA	GGGAAGCATTTCTG	CATAATGAGGAGC
	CATGCAAGG	CAAGCTC	AAGCACATGG

10 most likely off-target sites of each sgRNA were generated at http://crispor.tefor.net/crispor.py.

Letters in red indicate bases different from those of the target sequences.

Table S1d. Primers designed for Genotype Identification.

Primer	Sequence (5' to 3')	Target Size
Nphp1-KO-F	TACACAGTCGTGCCAGCCAG	~476bp
Nphp1-KO-R	GCTCCACTCTTCAATGTGGGA	~476bp
Nphp1-WT-F	CTGGTCTACCATGACTGCGTG	~887bp
Nphp1-WT-R	GCTCCACTCTTCAATGTGGGA	~887bp

PCR primer pairs for genotype identification were designed at http://www.ncbi.nlm.nih.gov/tools/primer-blast/. The target sizes of *Nphp1*$^{del2\text{-}20/del2\text{-}20}$ and *Nphp1*$^{+/+}$ mice were expected to be approximately 476bp and 887bp, respectively.